SYMPATHETIC NERVOUS SYSTEM MODULATION OF CANCER VACCINE ACTIVITY, AND NANOPARTICLE DRUG DELIVERY FOR LIMB ISCHEMIA

A Dissertation

by

LOUIS EDWARD HINKLE

Submitted to the Graduate and Professional School of
Texas A&M University
in partial fulfillment of the requirements for the degree of

DOCTOR OF PHILOSOPHY

Chair of Committee,	David P. Huston
Co-Chair of Committee,	Haifa Shen
Committee Members,	Jenny Chang
	Sankar Mitra
	Xian Chang Li
Head of Program,	Carol Vargas Bautista

May 2023

Major Subject: Biomedical Sciences

ABSTRACT

The sympathetic nervous system (SNS) is an important regulator of immune cell function during homeostasis and states of inflammation. Recently, the SNS has been found to bolster tumor growth and impair the development of anti-tumor immunity. However, it is unclear whether the SNS can modulate antigen presenting cell (APC) function. In project 1, we investigated the effects of SNS signaling in monocyte-derived macrophages (moMΦ) and dendritic cells (DCs) and further combined the nonspecific β-blocker propranolol with a peptide cancer vaccine for the treatment of melanoma in mice. We report the novel finding that norepinephrine treatment dramatically altered moMΦ cytokine production and T cell priming, whereas DCs were unresponsive to norepinephrine and critically lack β_2-adrenergic receptor expression. In addition, we show that propranolol plus cancer vaccine enhanced peripheral DC maturation, increased the intratumor proportion of effector $CD8^+$ T cells, and decreased the presence of intratumor PD-$L1^+$ myeloid-derived suppressor cells. Furthermore, this combination dramatically reduced tumor growth compared to vaccination alone. Taken together, these results offer novel insights into the cell-specific manner by which the SNS regulates the APC immune compartment and provide strong support for the use of propranolol in combination with cancer vaccines to improve patient response rates and survival.

Occluded limb arteries require immediate revascularization, but return of blood flow causes additional tissue damage through generation of reactive oxygen species (ROS) and dysregulation of nitric oxide (NO) production. In project 2, we report a

hybrid molecule SA-10 with both NO donating and ROS scavenging abilities for the treatment of limb ischemia-reperfusion (I/R) diseases. SA-10 demonstrated potent cytoprotection and tube formation activity in endothelial cells under H_2O_2-induced oxidative stress. In addition, SA-10 loaded poly(lactic-co-glycolic acid) nanoparticles (SA-10 NPs) were delivered intramuscularly in two murine hindlimb ischemia models. In the acute I/R model, SA-10NP significantly reduced muscle damage, hyper inflammation, and lung edema. In the chronic ischemia model, SA-10 significantly improved blood perfusion and physical endurance over 30 days. Elderly patients with acute and chronic limb ischemia have limited options for surgical or endovascular interventions, so a therapeutic alternative to surgery such as SA-10NP is greatly needed.

ACKNOWLEDGEMENTS

I thank my committee chair, Dr. David Huston, my mentors Dr. Haifa Shen and Dr. Maham Rahimi, and my committee members Dr. Jenny Chang, Dr. Sankar Mitra, and Dr. Xian Li for providing excellent guidance throughout my graduate training.

Many thanks to the Houston Methodist Research institute (HMRI) Comparative Medicine Program for assistance in animal housing, maintenance, and monitoring. I additionally appreciate the resources and assistance provided by the Houston Methodist Flow Cytometry Core and the Houston Methodist Immunomonitoring Core.

Lastly, I would like to thank my family and friends for their patience, encouragement, and support.

CONTRIBUTORS AND FUNDING SOURCES

Contributors

This work was supervised by a thesis dissertation committee consisting of Professor David Huston (Chair, Department of Microbial Pathogenesis & Immunology Texas A&M College of Medicine), Professor Haifa Shen (Co-Chair, Department of Nanomedicine HMRI), Professor Jenny Chang (committee member, Cancer Center HMRI), Professor Sankar Mitra (committee member, Department of Radiation Oncology HMRI), and Professor Xian Li (committee member, Department of Surgery Houston Methodist).

Sample preparation and data analysis for Figures 7-10 and Figure 15 in Chapter 3 were provided by Duong Le and Tam Nguyen from the Department of Bioengineering, University of Texas at Arlington.

All other work conducted for the thesis was completed by the student independently.

Funding Sources

The work presented in Chapter 2 was supported by NIH grants U54CA210181 (to HS), R01CA193880 (to HS), and R01CA222959 (to HS). Additional funding sources include grants from HMRI (to S-HC) and the Emily Hermann endowed chair funds (to S-HC) as well as a trainee project grant under the U54CA210181 CITO (to LH).

The work presented in Chapter 3 was supported by the Applied Research Seed grant (2400018) (to SA) by UNTHSC, NIH grants R15HL156076 and T32HL134613 (to

KN), the George and Angelina Kostas grant (to MR and HS), and the 2020 Society for Vascular Surgery student fellowship awarded (to LH).

TABLE OF CONTENTS

Page

LIST OF FIGURES

Page

CHAPTER I

INTRODUCTION

Project 1: The sympathetic nervous system modulates cancer vaccine activity through monocyte-derived cells

Cancer patients experience increased sympathetic nervous system (SNS) tone from both overt autonomic nerve growth at the solid tumor as well as from the emotional stress that accompanies cancer diagnosis [1]. High autonomic nerve density in tumors is associated with worse prognosis and more aggressive characteristics in human prostate, breast, colon, and pancreatic cancers [2] [3] [4]. Additionally, inhibition of SNS signaling through β-blockers has been associated with improved prognosis in several types of cancers in human patients [5] [6] [7]. The SNS and its primary neurotransmitter norepinephrine stimulate the ubiquitously expressed adrenergic receptors to affect a wide range of biological functions, and SNS regulation of immune cells directly contributes to cancer progression and the effectiveness of cancer immunotherapy. Increased SNS signaling has been associated with decreased tumor infiltrating lymphocytes in several mouse models, and stimulation of β_2-adrenergic receptors (β_2ARs) on tumor-associated macrophages (TAMs) and myeloid-derived suppressor cells (MDSCs) increases their frequency in tumors and enhances their pro-tumorigenic functions [8] [9] [10] [11]. These preclinical findings indicate that combining β-blockers with immunotherapies could subvert tumor-mediated immune suppression to maximize patient immune responses. Interrupting sympathetic signaling through the use of β-blockers has the potential to improve cancer vaccine strategies, but the extent to which

the sympathetic nervous system impairs antigen presenting cell (APC) function, which is critical for vaccine efficacy, remains unclear. In the studies presented in chapter II, we explore the impact of sympathetic signaling on APC subsets and cancer vaccine activity. These studies reveal that the SNS regulates APCs in a cell specific manner. In addition, we provide support for the use of β-blockers to subvert tumor-mediated mechanisms of immune suppression and improve clinical responses to cancer vaccines.

Project 2: Nano encapsulated novel compound SA-10 with therapeutic activity in both acute and chronic murine hindlimb ischemia models

Peripheral ischemia occurs when one or more arteries in the extremities becomes blocked, which leads to reduced blood flow and subsequent tissue damage. This can occur in a chronic setting where arteries become gradually more occluded, often by progressive stenosis or atherosclerosis, until the disease reaches a critical state. Peripheral ischemia can also acutely occur during cardiogenic thromboembolism, *in situ* thrombosis, and vascular injury, which results in sudden decreases in limb perfusion that threatens limb viability and requires immediate diagnosis and revascularization. In both the chronic and acute settings of peripheral ischemia, return of blood flow is necessary to prevent tissue loss but paradoxically also induces further tissue damage. Ischemia-reperfusion (I/R) injury can result in tissue compartment swelling, endothelial cell dysfunction, and sterile inflammation. The molecular mechanisms that contribute to endothelial cell dysfunction and inflammation during I/R injuries are multifactorial, but the dysregulation of nitric oxide (NO) production as well as sudden return of oxygen and generation of reactive oxygen species (ROS) appear to be driving contributors.

We have previously reported the design of a hybrid molecule 4-amino TEMPOL-H sydnonimine (SA-2) that combines a pH-responsive NO donor and superoxide dismutase (SOD) mimetic functional groups [12]. SA-2 improved endothelial cell viability and function under oxidative stress and alleviated ROS levels *in vitro*, which suggests it is a promising candidate drug for treatment of I/R injury [13]. Here, we report the second generation of hybrid ROS/NO donor drug for I/R injury treatment SA-10. Structure activity optimization of the SA-2 molecule led to the more potent hybrid compound (WO/2020/132496) SA-10 containing sulfone functional groups. We report that SA-10 exhibited superior *in vitro* cytoprotective, angiogenic, and endothelial NO synthase (eNOS) upregulating activities compared to SA-2. We additionally report that SA-10 packaged in poly(lactic-co-glycolic acid) PLGA nanoparticles (SA-10NPs) dramatically mitigated tissue damage, local inflammation, and muscle function in murine models of chronic and acute ischemia injury. Ultimately, nanoparticle delivery of SA-10 could greatly benefit patients who suffer from acute and critical limb ischemia. Many elderly patients who suffer from acute limb ischemia cannot undergo surgical or endovascular interventions, so SA-10 NPs fill an important need towards the development of therapeutic alternatives to surgery for the treatment of ischemia diseases.

CHAPTER II

PROJECT 1: THE SYMPATHETIC NERVOUS SYSTEM MODULATES CANCER VACCINE ACTIVITY THROUGH MONOCYTE-DERIVED CELLS*

Introduction and Literature Review

The SNS is an important regulator of immune cell function both during states of inflammation and under homeostasis [14]. Postganglionic fibers of sympathetic nerves innervate bone marrow and secondary lymph organs to regulate circadian patterns of leukocyte recruitment to tissues [15]. Additionally, sympathetic nerve terminals that innervate the paracortex zones of lymph nodes will release catecholamines during states of inflammation to regulate innate and adaptive immune cell function largely through β_2AR signaling [14] [16] [17]. The β_2AR is a G protein-coupled receptor (GPCR) that induces G protein activation, increased cAMP, PKA activation, and phosphorylation of cAMP response element-binding protein (CREB) through one of its major signaling pathways when stimulated [18]. It is becoming increasingly clear that SNS signaling contributes to tumor progression through its suppressive effects on tumor immunity [1]. Growth of intratumor sympathetic nerves has been reported to be critical for the growth of several types of human and murine tumors [2] [3] [19] [20], and reversal of SNS signaling through the use of β-blockers has improved human cancer patient outcomes [5] [6] [7]. Targeting SNS signaling through the use of β-blockers has great promise as a

*Reprinted with permission from "The Sympathetic Nervous System Modulates Cancer Vaccine Activity through Monocyte-Derived Cells" by Louis Hinkle, Yongbin Liu, Chaoyang Meng, Zhe Chen, Junhua Mai, Licheng Zhang, Yitian Xu, Ping-Ying Pan, Shu-Hsia Chen, Haifa Shen. 2021. Journal of Immunology, 207(12), 3131-3140, Copyright 2021 by The American Association of Immunologists, Inc.

combination treatment with cancer immunotherapies, but much remains to be understood in the role of SNS and the development of tumor immunity. For this reason, this literature review will examine our current knowledge into the connection between SNS signaling and tumor progression as well as SNS control of immunity

Sympathetic nerve innervation in tumors

Tumor growth was initially linked to the nervous system due to the observation that cancer cells have a predilection to grow along nerve fibers in a process termed perineural invasion [21]. Now, it is well understood that sensory and autonomic nerve fibers are present in multiple types of human tumors and that higher nerve density can be associated with worse prognosis [22] [4] [3] [23]. Claire Magnon and her colleagues helped elucidate the extent to which nerves influence the tumor microenvironment by showing that both sympathetic and parasympathetic nerves actively invade and form new nerve fibers in prostate tumors to support tumor growth [2]. Chemical or surgical ablation of sympathetic nerves at the primary tumor site prevented the growth of primary prostate tumors as well as the formation of metastatic lesions. Additionally, blockade of parasympathetic signaling mitigated the dissemination of prostate tumor cells and the formation of metastases [2]. Similar to the findings presented by Magnon et al., denervation of intratumor sympathetic nerves have been reported to mitigate the growth of several murine models of breast, lung, and head and neck cancers [19] [24] [11] [20]. However, denervation of parasympathetic nerves has been reported to either accelerate or diminish tumor growth depending on the tumor model studied. Surgical transection of the vagus nerve and blockade of cholinergic signaling increased the growth rate of

pancreatic cancer in mice [25] [26]. On the other hand, surgical or pharmaceutical blockade of parasympathetic signaling reduced the growth of gastric and prostate cancers [27] [2]. While the impact of cholinergic signaling on tumor growth is tissue type dependent, sympathetic signaling appears to universally benefit tumor growth. However, the extent to which sympathetic nerves control tumor growth via its influence on tumor cells or indirect effects on stromal and immune cells is still being explored.

Tumor angiogenesis

Early mechanistic insights into sympathetic control of tumor growth comes from murine cancer models that connect β_2AR signaling and enhanced angiogenesis and tumor growth [28] [29]. The switch to a highly angiogenic state occurs early in tumor development and is necessary for exponential growth [30]. Zahalka et al., revealed that mice lacking endothelial β_2AR expression were unable to achieve exponential prostate tumor growth due to impaired angiogenesis [31]. Loss of β_2AR expression on endothelial cells resulted in increased oxidative phosphorylation at the expense of reduced aerobic glycolysis, which is necessary for angiogenesis [31]. Similar findings were reported in murine models of lung, ovarian, and breast cancer where chemical ablation of sympathetic nerves mitigated tumor neovascularization, and chronic stress increased tumor growth and vascularization [11] [28] [29]. Sympathetic control of neovascularization in lung and breast cancer models were in part mediated through altered tumor-associated macrophage (TAM) production of vascular endothelial growth factors (VEGFs) [11] [29]. On the other hand, increased ovarian cancer vascularization in stressed mice was reported to be controlled by stimulation of β_2ARs on cancer cells

leading to increased production of VEGFs [28]. Similar to its effects on tumor blood vasculature, sympathetic signaling has been reported to promote lymphangiogenesis and ultimately tumor cell dissemination in murine breast cancer [32]. The increase in intratumor lymph vessel dilation resulted from increased recruitment of TAMs, which in turn induced expression of VEGFs from tumor cells and stromal cells to influence lymph vessel changes [32]. Together, these studies show that sympathetic signaling promote tumor progression through changes to intratumor blood and lymph vasculature. It is unclear whether β_2AR signaling at tumor cells, TAMs, or stromal cells individually govern these changes to vessel formation. Instead, changes to tumor vasculature is likely due to pleiotropic effects of sympathetic signaling at each of these cell types.

Cancer cell biology and therapy resistance

In addition to SNS alteration of the tumor microenvironment, several protumorigenic changes to cancer cell biology has been attributed to increased sympathetic signaling including oncogene activation, increased survival pathways, and impaired DNA damage repair. Norepinephrine stimulation of β_2ARs has been reported to activate the Src oncogene pathway in human ovarian cancer cell lines to increase cell migration and invasion *in vitro* as well as tumor growth *in vivo* [33]. β_2AR signaling directly supports tumor growth through Src and FosB-dependent mechanisms that increase IL-6 and IL-8 production from human ovarian cancer cells, respectively [34] [35]. β_2AR signaling has also been found to increase transcription of the Her2 oncogene in human breast cancer cell lines, which in turn creates a positive feedback loop of increased catecholamine production and autocrine signaling to ultimately enhance cancer

cell proliferation [36]. In addition, increased β_2AR signaling contributes to enhanced breast cancer cell survival through its downstream signaling protein protein kinase A (PKA), which contributes to trastuzumab resistance in $Her2^+$ breast cancer cell lines through its interaction with Akt dephosphorylation [36] [37]. Furthermore, β_2AR expression on cancer cells can also promote tumor progression through increased accumulation of DNA damage due to impaired DNA repair mechanisms. β_2AR expression on human osteosarcoma and somatic cell lines was mechanistically linked to p53 degradation and accumulation of DNA damage through downstream G-protein and β-arrestin signaling pathways [38]. β_2AR expression on human breast cancer cells lines similarly resulted in increased DNA damage that enhanced tumorigenicity and conferred resistance to paclitaxel treatment *in vivo* [39]. Based on these findings, sympathetic nerves and β_2AR activation contributes to tumor progression due to their influence on multiple physiological pathways at both cancer cells and stromal cells in the tumor microenvironment. Sympathetic nerve density and catecholamine content in tumors therefore hold important implications for disease prognosis as well as patient response to therapy.

Sympathetic control of tumor immunity

It is well appreciated that chronic, stressful psychosocial factors and upregulation of circulating catecholamines have broad immunosuppressive effects [40], but the extent to which neuroimmune crosstalk affects cancer progression is unclear. Sympathetic nerve innervation of the tumor microenvironment could directly impact tumor infiltrating lymphocytes as well as intratumor myeloid cell populations. Additionally,

sympathetic nerves are known to innervate lymph nodes and spleen tissues to regulate inflammation and adaptive immune responses [41], and systemic increases in sympathetic tone that occur during tumor growth could impact the development of antitumor immunity at these secondary lymph organ sites. The possibility of crosstalk between sympathetic nerves and immune cells have important implications for the thriving field of cancer immunotherapy, which aims to bolster a patient's immune response to their tumor.

Myeloid cells and innate immunity

Tumors can avoid immune detection through the accumulation of myeloid cell populations, which include macrophages, dendritic cells, and MDSCs, that take on immunosuppressive functions [42]. MDSCs are immature myeloid cells that express Cd11b and Gr-1 and exhibit suppressive activity through high expression of arginase, prostaglandin E_2, and anti-inflammatory cytokines [42]. Mohammadpour et al., discovered that β_2AR signaling on the surfaces of MDSCs increases their frequency, survival, and immunosuppressive molecule production in breast cancer tumor microenvironments in mice [43]. They additionally found that culturing human peripheral blood mononuclear cells (PBMCs) with a β_2AR agonist resulted in increased MDSC differentiation and expression of the immunosuppressive molecules arginase-I (ArgI) and PD-L1 [43]. Similar to MDSCs, TAMs contribute to tumor immune evasion through production of immunosuppressive molecules and promotes tumor progression by promoting angiogenesis and cancer cell extravasation [44]. Xia et al., found that blockade of sympathetic signaling minimized murine lung tumor neovascularization and

growth through reduced TAM function [11]. Consistent with this *in vivo* finding, catecholamines polarized macrophages towards an M2, immunosuppressive phenotype with increased VEGF production and endothelial tube formation activity *in vitro* [11]. Sloan et al., similarly found that enhanced β-adrenergic signaling promoted TAM tumor invasion, which in turn caused increased tumor cell extravasation and metastasis in a murine model of breast cancer [29]. Other *In vitro* studies have also revealed that macrophages polarize towards an M2 phenotype and exhibit increased production of immunosuppressive molecules when exposed to norepinephrine or other β-adrenergic agonists [45] [46]. These findings show that sympathetic innervation of tumors influence intratumor myeloid populations towards protumorigenic functions that might undermine immune-based cancer therapies.

T lymphocyte function

Cytotoxic T cells are often key to immune rejection of tumor growth, and there is increasing evidence that catecholamines will impair T cell priming and function both in the tumor microenvironment and at secondary lymph organs. Under homeostasis conditions, sympathetic nerves innervate spleen and lymph node tissues at areas rich in naïve T cells and APCs and will release norepinephrine within hours of antigen presentation and recognition [41] [16] [17]. Naïve $CD4^+$ T cells exclusively express the β_2AR, but will differentially upregulate or downregulate β_2AR expression following differentiation into helper T cell subsets [47]. Type 1 helper T cells (T_H1 cells) dramatically increase their expression of β_2AR compared to naïve $CD4^+$ T cells, and norepinephrine treatment of T_H1 cells results in lowered IL-2 production and reduced

cell proliferation and survival [48]. On the other hand, differentiation into T_H2 cells leads to downregulation and loss of β_2AR, leaving them unaffected by norepinephrine treatment [48]. These findings suggest that sympathetic nerves will polarize the $CD4^+$ T cell compartment away from a T_H1 profile, which typically supports the priming of cytotoxic, type 1 immunity, and instead towards a T_H2 profile, which is associated with increased IL-10 and immune tolerance [47]. Daher et al., found that naïve $CD8^+$ T cells also express β_2AR and downregulate the receptor after T cell receptor stimulation [49]. When exposed to norepinephrine or other β_2AR agonists, naïve $CD8^+$ T cells produce less IL-2 and exhibit reduced proliferation, similar to its effects on T_H1 cells [49]. Consistent with these *in vitro* findings, Daher et al., also found that treatment of mice with a β-blocker prior to treatment with a cancer vaccine reduced $CD8^+$ T cell priming in lymph nodes [49]. Another group similarly found that increased sympathetic signaling reduces $CD8^+$ T cell priming following influenza infection but suggested that changes to T cell priming were due to sympathetic influence on APCs rather than direct influence on T cells [50]. Taken together, these studies show that catecholamines from sympathetic nerves can affect $CD4^+$ and $CD8^+$ T cell priming *in vitro*, and that *in vivo* changes to T cell priming likely results from the combined effects of β-adrenergic signaling at T cells as well as at APCs.

Dendritic Cells and other APCs

Increased sympathetic signaling has been associated with altered T cell priming *in vivo* [50] [49], and it is likely that catecholamine influence on APCs contributes to this effect [50]. While there has been much study into the immunosuppressive effects of

β_2AR signaling on cytokine production in innate immune cells such as macrophages and monocytes [51] [45], the extent to which catecholamines regulate APC function remains unclear. During inflammatory events, lymph node resident conventional dendritic cells (cDCs), migratory cDCs, and inflammatory monocytes-derived cells (MCs) will migrate together deep into the T cell-rich paracortex region of lymph nodes to modulate T cell responses [52] [53] [54]. cDCs and MCs are APCs that contribute to T cell priming through their influence on the local inflammatory milieu and antigen presentation, and they exhibit nonoverlapping function depending on the inflammatory trigger [52] [53] [55]. Catecholamine-mediated suppression of APC function could undermine anti-tumor immunity if it sufficiently affects APC priming of cytotoxic T cells. For these reasons, it is critical to understand how sympathetic signaling regulates these APC subsets in order to overcome it as a potential barrier to cancer immunotherapy strategies.

Current understanding into SNS control of APC function is derived from indirect evidence obtained from *in vivo* studies and from sparse *in vitro* studies that utilize bone marrow-derived DCs (BMDCs). Kokolus et al., discovered that chronically stressed mice, which results in increased circulating catecholamines and glucocorticoids, have increased proportions of immature DCs [56]. However, this study is limited by the fact that they did not specifically examine the influence of sympathetic signaling over glucocorticoid responses. Additionally, the authors identified DCs by high expression of CD11c, which is a nonspecific marker that also includes some macrophages and MCs. Grebe et al., more directly evaluated the impact of sympathetic signaling on DCs and other APCs using chemical denervation drugs and β-blockade in murine models of

influenza infection [50]. The authors found that loss of sympathetic signaling impaired priming of $CD8^+$ T cells following influenza infection dependent on host APC function. Further investigation revealed that peritoneal APCs and peritoneal DCs had enhanced T cell priming abilities after sympathetic nerve denervation, and that catecholamines rely on β_2ARs to exert their effect [50]. This study was limited by the indirect nature in which DCs were implicated in SNS control of $CD8^+$ T cell priming. While the authors showed that APCs and DCs were responsible for changes to T cell priming after changes to sympathetic signaling, they did not show that β_2AR expression on these cells specifically mediated these effects. They additionally found that norepinephrine treatment of isolated CD8α DCs did not impact IL-12p40 production *ex vivo*, which either suggests that SNS control of DCs is indirect, or does not rely on IL-12 [50].

More direct evidence of SNS control of APCs comes from *in* vitro studies that evaluated β_2AR signaling in BMDCs. BMDCs are commonly used to study DC biology and were originally assumed to represent a homogenous DC population [57] [58]. However, recent transcriptomic and functional analyses have revealed that $CD11c^+MHCII^+$ BMDCs are actually a group of heterogeneous cells arising from common DC precursors (CDPs) and common monocyte precursors (cMoPs) that remain distinct cell types after stimulation with lipopolysaccharide (LPS) [59] [60]. The spontaneously mature $CD11c^+MHCII^{hi}$ BMDCs that arise from CDPs are functionally and transcriptionally similar to migratory DCs, whereas the semi mature $CD11c^+MHCII^{int}$ BMDCs that arise from cMoPs most closely resemble macrophages [59]. Thus, BMDC cultures include a mixture of DCs and monocyte-derived

macrophages (moMΦ), which reflects the complex APC compartment present in lymph nodes during states of inflammation and immunization.

Through evaluation of β_2AR agonist-treated BMDC cultures, it has been previously reported that β_2AR signaling impairs DC priming of T_H1 cells through reduced IL-12p70 and increased IL-10 production [61] [62]. Norepinephrine mediates this effect through reduced NF-κB activation in BMDCs, but the molecular pathways that mediate β_2AR interaction with NF-κB are still unclear [61] [63]. BMDC cultures have additionally been used to support claims that β_2AR expression on DCs and SNS control of DC cytokines are involved in the pathogenesis of rheumatoid arthritis [64]. However, these studies did not account for BMDC heterogeneity and the presence of moMΦ, which likely contribute to the observed effects of β_2AR signaling [59].

In the studies presented in this chapter, we separated BMDC populations based on their expression of the macrophage-colony stimulating factor receptor CD115, which is exclusively expressed on moMΦ, and evaluated DC and moMΦ responsiveness to norepinephrine to better understand how the SNS regulates the APC immune compartment. We additionally investigated the benefit of combining the nonspecific β-blocker propranolol with a peptide-based cancer vaccine in mounting anti-tumor immune responses. A murine model of B16 melanoma with ovalbumin (OVA) expression was chosen for this study since it has previously been shown that βAR signaling is relevant both systemically and intratumorally in mice bearing this tumor type [65] [66]. B16-bearing mice were vaccinated with a combination of the OVA peptide SIINFEKL and the adjuvant polyinosinic-polycytidylic acid (Poly IC)

complexed with poly-L-lysine (Poly ICLC). Poly IC is a synthetic double-stranded homopolymer that stimulates TLR3, which normally recognizes double-stranded RNA to induce TRIF-dependent signaling [67]. When complexed with poly-L-lysine to form Poly ICLC, Poly IC has improved stability in serum and enhanced proinflammatory properties [68]. Poly ICLC is commonly used in vaccine design and has proven to be effective in cancer vaccine clinical trials [67]. In summary, our work offers insight into catecholamine-mediated regulation of DCs and moMΦ as well as provides supports for the use of β-blockers to subvert tumor-mediated mechanisms of immune suppression. This study also highlights the need to delineate the heterogeneous populations in BMDC cultures when studying DC biology.

Materials and Methods

Cell lines

Murine melanoma cancer cell line B16 that stably expresses OVA was a gift from Dr. Kenneth Rock, Dana-Farber Cancer Institute, Boston. B16-OVA cells were cultured in DMEM supplemented with 10% fetal bovine serum (FBS, GenDEPOT) + 1x 2-mercaptoethanol (BME) + 1:100 penicillin and streptomycin (PS, GenDEPOT). Cells were maintained in a cell incubator at 37°C under 5% CO_2.

Generation of bone marrow-derived dendritic cells

BMDCs were generated by culturing C57BL/6J mouse bone marrow cells in GM-CSF for 10 days. Briefly, four to eight-week-old C57BL/6J mice were sacrificed and femur and tibia bones were dissected and cleaned. Bone marrow cells were flushed and plated on 100 mm^2 tissue culture dishes at 2 million cells per dish in 10 mL of

complete BMDC media consisting of 1640 RPMI + 10% FBS (GenDEPOT) + 1x BME + 1:100 PS (GenDEPOT) + 20 ng/mL GM-CSF (PreproTech). An additional 10 mL of complete BMDC media were added 3 days later, and 10 mL of media were removed and replaced with fresh complete BMDC media every 2 days until day 10. To separate BMDCs into $CD115^+$ and $CD115^-$ populations, a CD115 microbead kit was used according to the manufacturer's protocol (Miltenyi Biotec).

Vaccine preparation

Vaccines were composed of 4 mg/kg Poly ICLC, 100 μg of SIINFEKL peptide, and sterile phosphate buffered saline (PBS). Poly ICLC was created by mixing Poly IC (Sigma-Aldrich) with poly-l-lysine (Sigma-Adrich) in 2% carboxymethylcellulose/sterile PBS as previously described [68].

In vivo treatment

Four to eight-week-old female C57BL/6J mice were inoculated with 1.5×10^5 B16-OVA melanoma tumor cells in 30% Matrigel matrix (Corning) by subcutaneous flank injection. Mice were treated with propranolol and/or a vaccine according to schedules detailed in the results section. Propranolol hydrochloride (Sigma-Aldrich, 10 mg/kg, 100 μL) was administered via intraperitoneal injections. Vaccines were administered via 100 μL footpad injections. Tumors were measured with digital calipers, and tumor volumes were calculated as (Length×width×width)/2.

Enzyme-linked immune absorbent spot (ELISpot)

Spleens were isolated from tumor-bearing mice, crushed, and lysed with ammonium-chloride-potassium (ACK) buffer (Gibco). Cells were then centrifuged,

resuspended in RPMI + 10% FBS + 1x BME + 1:100 PS and filtered through 40 μm mesh filters (Greiner Bio-One). The resulting single cell suspensions were plated on a sterile ELISpot plate (Mabtech) that was previously coated with an IFN-γ capture antibody (Invitrogen) at 2×10^5 cells per well with 10 μg/mL SIINFEKL peptide and maintained at 37°C with 5% CO_2 supply for 48 hours. Then, the plate was washed with PBS, incubated with an IFN-γ detection antibody (Invitrogen) for 1 hour at room temperature, incubated with horse-radish peroxidase (Invitrogen) for 30 minutes at room temperature, and then color developed with AEC substrate (BD Biosciences). Once red dots were visible, color development was ceased by rinsing the plate with water. Images of the ELISpot plates and quantification of the dots were done using a digital ELISpot plate reader (Cellular Technology Limited).

Flow cytometry

Cells were incubated with antibodies in the dark on ice for 30 minutes and then washed with 2% FBS in PBS prior to analysis. DAPI was used to determine live and dead cells. Cells were analyzed by flow cytometry (BD FACS Fortessa), and data were analyzed with FlowJo v10.0 software. Gating for each cell type were performed as follows: $CD45^+CD11c^+MHCII^+CD64^-Ly6C^-$ for DCs; $CD45^+CD11c^+MHCII^+CD64^-Ly6C^-CD8^+$ for $CD8^+$ DCs; $CD45^+CD11c^+MHCII^+CD64^-Ly6C^-CD103^+$ for CD103 DCs; $CD45^+CD11c^+MHCII^+CD64^-Ly6C^-B220^+$ for pDCs; $CD45^+CD11c^+MHCII^+CD64^-Ly6C^-CD11b^+$ for $CD11b^+$ DCs; $CD45^+CD11b^+CD64^+Ly6C^-$ for macrophages; $CD11b^+CD11c^+MHCII^+CD64^+$ for moDCs.

Time of flight cytometry (CyTOF)

To process tumor samples for CyTOF, tumors were dissected, rinsed with PBS, minced with a scalpel, and digested in 1640 RPMI + 1:100 PS + 400 U/mL DNase-1 (Simga) at 37°C for 45 minutes. The digested tumors were centrifuged at 500×g for 5 minutes, and then the cell pellets were resuspended in PBS. Hematopoietic cells were enriched from the cell suspension using 50/85% Percoll density gradient centrifugation. Briefly, 3 mL of cell suspension were transferred to 15 mL conical tubes and 5 mL of 50% percoll were carefully added to the bottom of the tube followed by 5 mL of 85% Percoll. The samples were then centrifuged at 1800×g for 30 minutes. The resulting cell layers between 50% and 85% Percoll were collected and washed with 2% FBS in PBS prior to staining procedures for CyTOF.

For CyTOF analysis, cells were stained with metal-tag viability dye for 5 minutes, washed with cell staining buffer (Fluidigm), and then stained with surface and intracellular markers based on a protocol for Foxp3 staining (eBioscience). Afterwards, cells were stained with Cell ID Intercalator Ir (Fluidigm) at 4°C overnight. Then, cells were washed with cell staining buffer and samples were acquired with Helios (Fluidigm). The results were analyzed with the CyTOF acquisition software and uploaded to Cytofbank for analysis. Each marker readout was normalized using a bead-based normalization algorithm, and beads and dead cells were gated out in the analysis step. Sub-populations of cells were analyzed with FlowJo and viSNE analysis was performed to generate tSNE plots. Gating for each cell type were performed as follows: $CD45^+CD3^+CD8^+$ for $CD8^+$ T cells; $CD45^+CD3^+CD8^+CD44^+CD62L^-$ for $CD8^+$ T_{EM};

$CD45^+CD3^+CD8^+CD44^+CD62L^+$ for $CD8^+$ T_{CM}; $CD45^+CD3^+CD4^+$ for $CD4^+$ T cells; $CD45^+CD3^+CD4^+CD44^+CD62L^-$ for $CD4^+$ T_{EM}; $CD45^+CD3^+CD4^+CD44^+CD62L^+$ for $CD4^+$ T_{CM}; $CD45^+CD11b^+Ly6C^+$ for M-MDSCs; $CD45^+CD11b^+Ly6G^+$ for PMN-MDSCs; $CD45^+CD11b^+Ly6C^-F4/80^+$ for TAMs; $CD45^+CD11b^+Ly6C^-F4/80^+CD206^+$ for M2 TAMS; $CD45^+CD11b^+Ly6C^-F4/80^+CD86^+$ for M1 TAMs; $CD45^+CD11C^+MHCII^+Ly6C^-CD64^-$ for DCs; $CD45^+B220^+$ for B cells.

Enzyme-linked immunosorbent assay (ELISA)

Supernatant from BMDCs were collected 18 hours after treatment and IL-10, IL-12p70, IFN-α were measured using ELISA cytokine measurement kits from ThermoFisher Scientific.

Western blotting

Protein was collected from BMDCs using RIPA buffer supplemented with protease and phosphatase inhibitors (1:100, GenDepot) at 4°C for 30 minutes with agitation. Samples were centrifuged at 13,000 x g for 20 minutes, supernatant was collected, and protein concentration was measured using a BCA protein assay kit. 10 μg of protein from each sample were separated by 10% SDS-PAGE and transferred onto nitrocellulose blotting membranes. Membranes were blocked with 5% nonfat milk, incubated with primary antibodies overnight, incubated with secondary antibody for 1 hour, and then developed using a chemiluminescent substrate (Thermo Fisher). Signal from the membranes were captured by X-ray films and a Medical Film Processor. Antibodies targeting phosphorylated CREB (Ser133), total CREB, and GAPDH were purchased from Cell Signaling Technologies.

RNA extraction and real-time quantitative PCR

Total RNA was extracted using PureXtract RNAsol RNA isolation solution (GenDEPOT). cDNA Reverse Transcription kit (Thermo Fisher) was used to convert total RNA to cDNA, and quantitative RT-PCR was performed using SYBR^{TM} Green Master Mix (Thermo Fisher) and StepOnePlus^{TM} Real-Time PCR system (GE Healthcare). Forward β_2AR primer: 5'-GGGAACGACAGCGACTTCTT-3'; Reverse β_2AR primer: 5'-GCCAGGACGATAACCGACAT-3'; Forward GAPDH primer: 5'-CATGGCCTTCCGTGTTCCTA-3'; Reverse GAPDH primer: 5'-TACTTGGCAGGTTTCTCCAGG-3'. Data was analyzed using the -2ΔΔct method such that β_2AR mRNA expression was normalized to GAPDH expression in each sample, and then fold change of CD115$^-$ DC β_2AR was calculated relative to CD115$^+$ moMΦ within each biological replicate.

Intracellular cAMP measurement

To measure intracellular cAMP, 5×10^5 cells were plated on 96 well plates and treated with 500 μM 3-Isobutyl-1-methylxanthine (IBMX, Sigma-Aldrich) and 100 μM Ro 20-1724 (Sigma-Aldrich) for 15 minutes. Then, the indicated groups were treated with 1 μM norepinephrine for 30 minutes. cAMP in these cells were then detected using the cAMP-Glo Max Assay kit (Promega).

T cell proliferation assay

To evaluate BMDC stimulation of T cell proliferation, OVA-specific CD8$^+$ T cells (OT-Is) were isolated from transgenic mice using a CD8$^+$ T cell negative isolation kit (Stemcell) and stained with Carboxyfluorescein succinimidyl ester (CSFE) according

to manufacturer protocol (ThermoFisher CellTrace™ CFSE Cell Proliferation Kit). CSFE-stained OT-I cells were then cocultured with $CD115^+$ or $CD115^-$ BMDCs that were previously treated with 100 nM SIINFEKL peptide and 60 μg/mL Poly ICLC with or without 1 μM norepinephrine at a ratio of 5:1 (OT-I:BMDC) for 48 hours at 37°C. OT-I total cell number and CSFE status was then evaluated via flow cytometry and cell counting beads mixed into each sample (Thermofisher).

Statistical analysis

Data were expressed as mean ± standard deviation. Statistical analysis for experiments with multiple groups was assessed using ANOVA followed by post hoc Tukey multiple comparison tests in GraphPad Prism 8 version 1.2. Two-tailed student T test was used to compare two groups in Figure 2D. Differences that were statistically significant are denoted by asterisks such that * $p < 0.05$, ** $p < 0.01$, and *** $p < 0.001$.

Study approval

Animals were purchased from Charles River Laboratories and maintained in barrier animal facilities approved by the American Association for Accreditation of Laboratory Animal Care (AAALAC) and in accordance with current regulations and standards of the United States Department of Agriculture, Department of Health and Human Services, and National Institutes of Health. All studies related to animals including housing, tumor inoculation and growth, and treatment were conducted under the approval of Houston Methodist affiliated IACUC.

Results

IL-10 contributes to norepinephrine suppression of BMDC pro-inflammatory cytokine production and maturation

Similar to previous studies that examined norepinephrine treated BMDCs, we found that norepinephrine pretreatment of BMDCs resulted in large, dose-dependent increases in IL-10 production following Poly ICLC treatment as well as concomitant decreases in IL-12p70 and IFN-α (Figure 1a, b, c). IL-10 is known to independently control DC inflammation responses in skin, lung, and gut tissues as well as in *in vitro* cultures [69] [70] [71] [72]. Additionally, IL-10 is known to directly regulate transcription of the IL-12p40 subunit [46], so we hypothesized that the increase in IL-10 following norepinephrine treatment contributes to reduced BMDC inflammatory responses. To test this hypothesis, we treated BMDCs with norepinephrine, TLR agonists, and increasing doses of a neutralizing IL-10 antibody. Depletion of active IL-10 in BMDC cultures abolished norepinephrine reduction of IL-12p70 and IFN-α secretion following Poly ICLC treatment (Figure 1b, c). Inclusion of the neutralizing IL-10 antibody also completely relieved norepinephrine suppression of BMDC IL-12p70 production after treatment with the TLR agonists LPS and CpG, which suggests that norepinephrine reliance on IL-10 holds true for other TLR agonists (Figure 1d). Additionally, we found that inclusion of the neutralizing IL-10 antibody allowed BMDCs to maximally express CD86 and CD80 costimulatory molecules after Poly ICLC treatment even in the presence of norepinephrine (Figure 1e, f). Taken Together, these results suggest that IL-10 greatly contributes to norepinephrine control of BMDC

function, and that norepinephrine stimulation of β_2ARs likely indirectly affect proinflammatory cytokines through immunosuppressive mediators, such as IL-10.

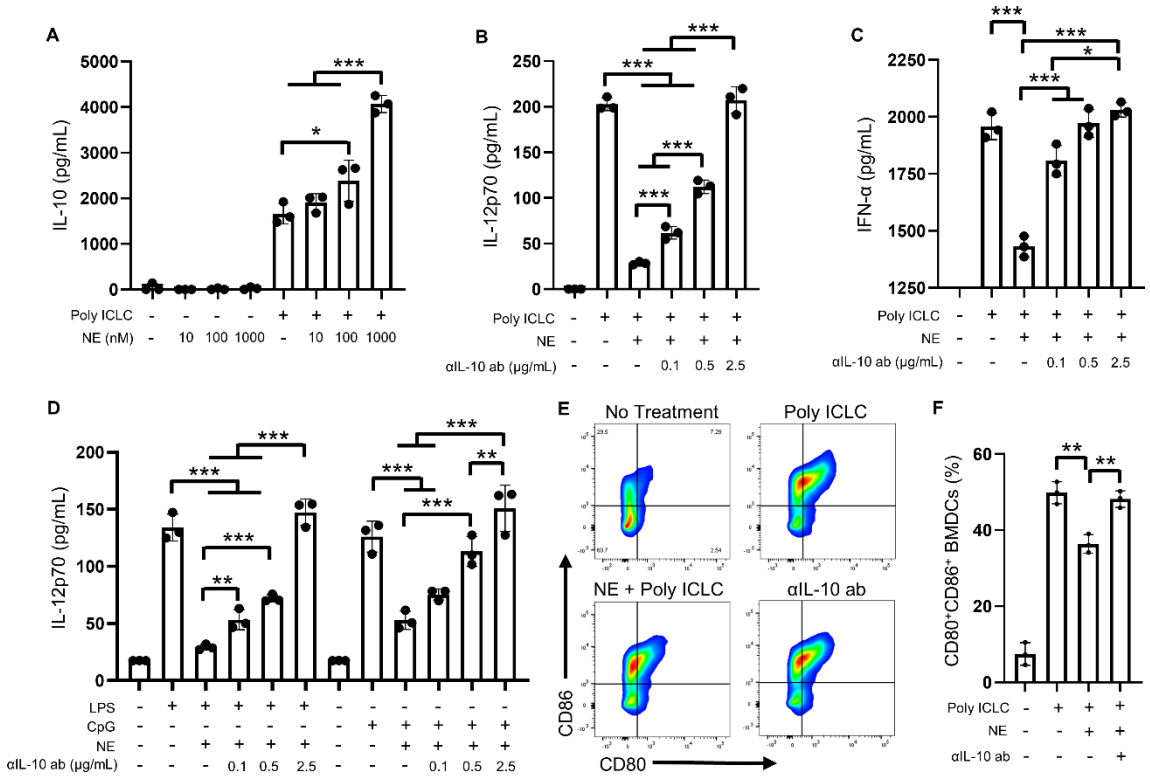

Figure 1.IL-10 contributes to norepinephrine suppression of BMDC pro-inflammatory cytokine production and maturation: BMDCs were pretreated with 1 μM (or indicated concentration) norepinephrine (NE) for 1 hour, then treated with 60 μg/mL poly ICLC, 100 ng/mL LPS, 500 ng/mL CpG, and/or 2.5 μg/mL (or indicated μg/mL concentration) neutralizing IL-10 antibody (αIL-10 ab), and culture supernatant were evaluated for A) IL-10, B&D) IL-12p70, and C) IFN-α 18 hours after treatment via ELISAs. E&F) BMDC expression of CD80 and CD86 costimulatory surface markers were evaluated by flow cytometry 18 hours after the indicated treatments. n = 3 technical replicates/group for A-F, and ANOVA followed by Tukey HSD post hoc tests were performed.

$CD115^+$ moMΦ in BMDC cultures, but not $CD115^-$ DCs express functional β2AR

Since IL-10 contributes to norepinephrine control of BMDC inflammation, and β_2AR signaling is known to promote IL-10 production from macrophages and monocytes [45] [73], we sought to delineate the individual cytokine contributions from DCs and other non-DC myeloid cells in BMDC cultures following norepinephrine treatment. Consistent with previous reports describing heterogeneity in BMDC cultures, we found that $CD11c^+MHCII^{int}$ BMDCs express CD115, whereas $CD11c^+MHCII^{hi}$ BMDCs lack expression of CD115 (Figure 2a). Using a CD115 magnetic microbead kit, we separated BMDCs into $CD115^-$ and $CD115^+$ populations that correspond with DC and moMΦ, respectively. After separation, $CD115^-$ BMDCs were loosely adhered, round cells that commonly presented fine dendritic protrusions that are characteristic of DCs (Figure 2c). On the other hand, $CD115^+$ BMDCs firmly attached to their surfaces and exhibited wide leading-edge lamellar protrusions that are similar to macrophage morphology (Figure 2c). $CD115^-$ BMDCs also expressed higher levels of the DC specific molecules CD135, PD-L2, Zbtb64, and CD117 than $CD115^+$ BMDCs (Figure 2b) and were stronger inducers of OT-I T cell proliferation than $CD115^+$ BMDCs (Figure 3f, g). Based on these differences in cell morphology, DC-specific molecule expression, and T cell stimulation, magnetic bead separation of BMDCs based on CD115 expression is an effective method to separate authentic DCs from other non-DC myeloid cells. Going forward, we will term the $CD115^-$ BMDCs as DCs and the $CD115^+$ BMDCs as moMΦ. To evaluate whether norepinephrine differentially impacts $CD115^-$ DCs and $CD115^+$ moMΦ, we examined β_2AR expression as well as β_2AR downstream

signaling after incubation with norepinephrine. We discovered that $CD115^+$ moMΦ express 5-fold higher amounts of β_2AR mRNA than $CD115^-$ DCs (Figure 2d). Flow cytometry analysis also revealed that $CD115^+$ moMΦ express β_2AR on their surface, whereas β_2AR is undetectable on $CD115^-$ DCs (Figure 2e). To test signal transduction of β_2ARs in each of these cell types, we examined cAMP production and CREB phosphorylation following norepinephrine treatment. After 30 minutes of norepinephrine treatment, $CD115^+$ moMΦ produced approximately 19 nM cAMP, whereas $CD115^-$ DCs did not produce detectable amounts of cAMP after norepinephrine treatment (Figure 2f). Consistent with this, norepinephrine treatment resulted in much greater CREB phosphorylation in $CD115^+$ moMΦ compared to $CD115^-$ DCs (Figure 2g). To determine if DCs in mice lack β_2AR similar to our *in vitro* observations, we evaluated β_2AR expression on the surface of DCs, moDCs, and macrophages from C57BL/6J mouse popliteal lymph nodes and spleens via flow cytometry. Indeed, we found that while macrophages and moDCs exhibit a distinct fluorescence shift after incubation with a β_2AR antibody, β_2AR was undetectable on $CD8^+$ and $CD103^+$ cDCs, and pDCs and $CD11b^+$ DCs exhibited minimal expression of β_2AR (Figure 2h). In summary, these results show that $CD115^+$ moMΦ and $CD115^-$ DCs in BMDC cultures have different expression patterns of the β_2AR, and that these patterns of β_2AR expression correlate with *in vivo* populations of DCs, macrophages, and moDCs.

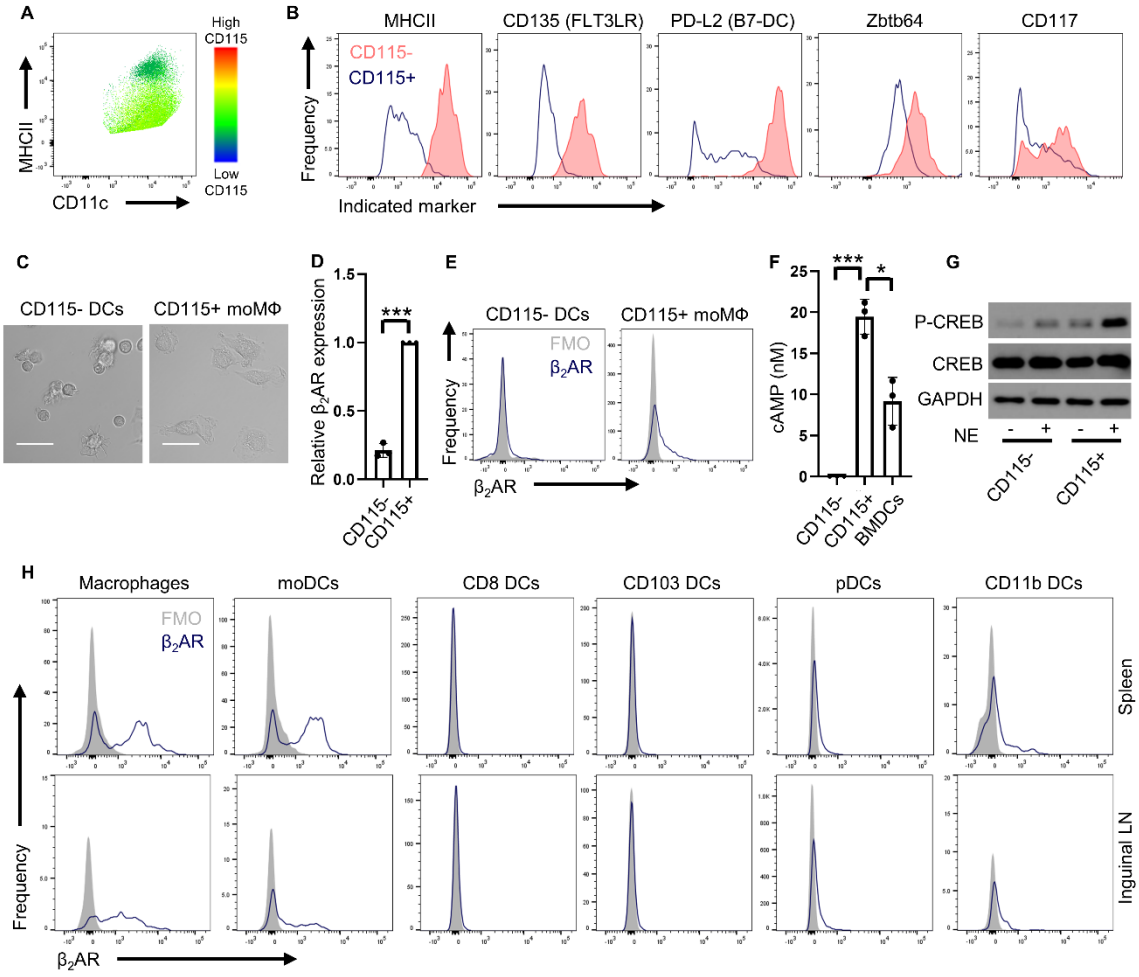

Figure 2. CD115$^+$ moMΦ, but not CD115$^-$ DCs in BMDC cultures express functional β_2AR: A) Flow cytometry analysis of CD11c$^+$MHCII$^+$ BMDCs with CD115 expression overlaid. CD115$^+$ and CD115$^-$ cells were separated from BMDCs using MACS microbeads and B) molecular markers were evaluated by flow cytometry, and C) cell morphology was evaluated by confocal microscopy (representative 60x images shown, scale bars = 30 μm). CD115$^+$ and CD115$^-$ cells were also evaluated for D) relative β_2AR mRNA expression via RT-PCR, E) surface β_2AR by flow cytometry, and F) cAMP production G) and CREB phosphorylation following norepinephrine treatment via

cAMP bioluminescent assay and western blot, respectively. H) β_2AR on the surfaces of macrophages, moDCs, and DCs from C57BL/6J mouse popliteal lymph nodes and spleens was evaluated via flow cytometry. n = 3 technical replicates/group for A-C and E-H, and n = 3 biological replicates/group for D. Representative groups shown for A-C, E, G, and H. ANOVA followed by Tukey HSD post hoc tests were performed for F, and two-tailed student's T test performed for D.

Norepinephrine alters cytokine secretion and T cell proliferation from CD115$^+$ moMΦ rather than from CD115$^-$ DCs

Following our discovery that CD115$^+$ moMΦ in BMDC cultures express more β_2AR and exhibit greater GPCR downstream signaling following norepinephrine treatment compared to CD115$^-$ DCs, we sought to delineate the individual contributions of CD115$^+$ moMΦ and CD115$^-$ DCs to cytokine production following norepinephrine treatment. After treatment with norepinephrine and Poly ICLC, CD115$^+$ moMΦ experienced an approximately 3.5 fold increase in IL-10 production, whereas CD115$^-$ DCs produced much less IL-10 after Poly ICLC treatment and did not significantly increase IL-10 following norepinephrine treatment (Figure 3a). This trend persisted after treatment of CD115$^+$ moMΦ and CD115$^-$ DCs with CpG and LPS. Only CD115$^+$ moMΦ significantly increased IL-10 production after treatment with norepinephrine and either CpG or LPS (Figure 3d). Norepinephrine also led to dramatically reduced IL-12p70 and IFN-α production from CD115$^+$ moMΦ following Poly ICLC treatment but did not reduce IL-12p70 and IFN-α production from CD115$^-$ DCs (Figure 3b, c). Similarly, norepinephrine diminished IL-12p70 production from CD115$^+$ moMΦ after

CpG or LPS treatment, but it did not affect $CD115^-$ DC production of IL-12p70 after TLR agonist treatment (Figure 3e). We additionally found that treatment of $CD115^-$ DCs with norepinephrine did not affect their ability to stimulate OT-I T cell proliferation, whereas norepinephrine treated $CD115^+$ moMΦ significantly reduced OT-I proliferation evident by decreased total OT-I T cells after coculture (Figure 3f, g). These results demonstrate that $CD115^+$ moMΦ are responsible for the changes to cytokine production in BMDC cultures and exhibit impaired T cell stimulation following norepinephrine treatment, whereas $CD115^-$ DCs in BMDC cultures are unaffected by norepinephrine after removal of $CD115^+$ moMΦ.

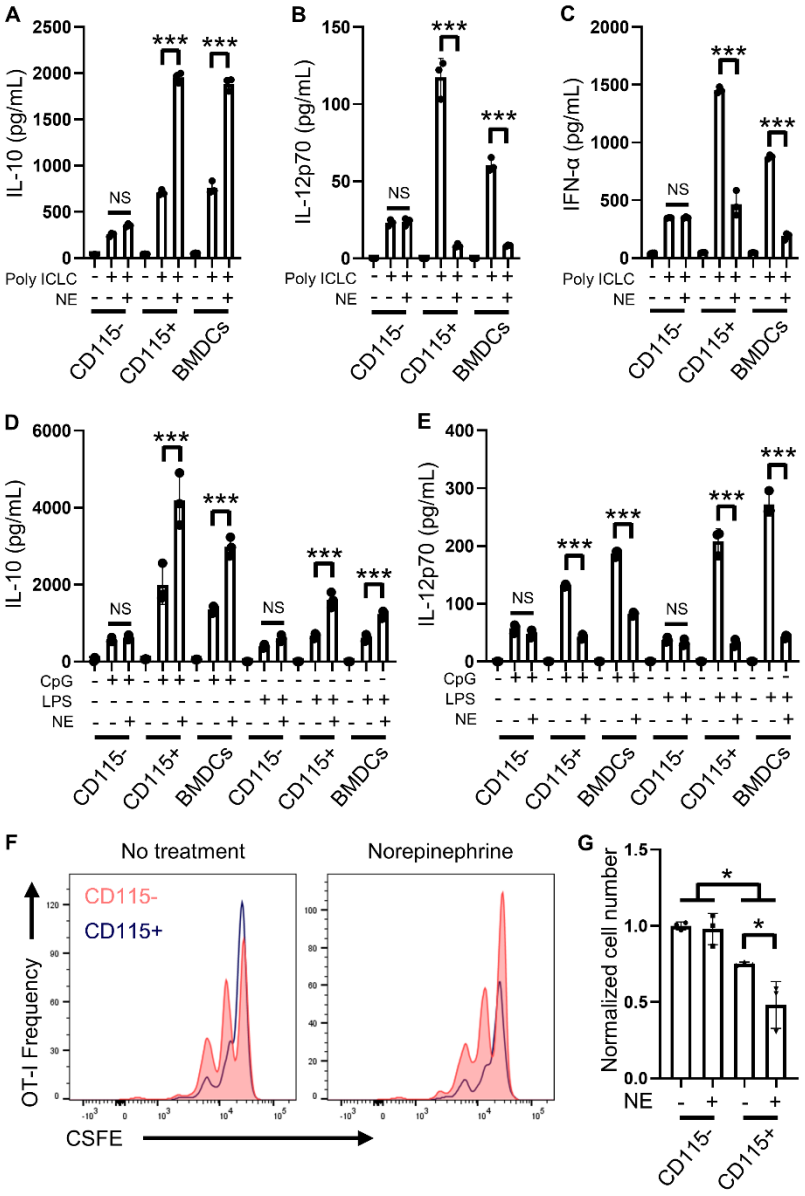

Figure 3. Norepinephrine alters cytokine secretion and T cell proliferation from CD115^{+} moMΦ rather than CD115^{-} DCs: CD115^{+} and CD115^{-} cells were separated from BMDCs using MACS microbeads and treated with 1 μM norepinephrine (NE), 60 μg/mL Poly ICLC, 100 ng/mL LPS, and/or 500 ng/mL CpG. 18 hours after the indicated treatments, A&D) IL-10, B&E) IL-12p70, and C) IFN-α from cell supernatant were

evaluated via ELISAs. F&G) T cell proliferation was evaluated by coculturing CSFE stained OT-I cells with $CD115^+$ or $CD115^-$ cells that were previously treated with 100 nM SIINFEKL and 60 μg/mL Poly ICLC with or without 1 μM norepinephrine at a ratio of 5:1 (OT-I:BMDCs). Representative histograms of OT-I CSFE fluorescence after 48 hour cocultures are shown in F, and total OT-I live cell number after 48 hour coculture normalized to OT-I + $CD115^-$ BMDCs without norepinephrine is shown in G. n = 3 technical replicates/group for A-G, and ANOVA followed by Tukey HSD post hoc tests were performed.

Propranolol enhances lymph node DC maturation following vaccination

Despite our finding that DCs do not express surface β_2ARs *in vitro* or *in vivo*, it has been reported that sympathetic signaling can diminish DC function *in vivo* [56] [50]. For this reason, we aimed to examine if inclusion of a β-blocker can improve DC responses to vaccination. We performed a therapeutic vaccine experiment according to the schematic in Figure 4a. The mice were then sacrificed on day 15, and lymph node, tumor, and spleen tissues were processed for flow cytometry analysis of DC surface costimulatory markers.

The combination of propranolol and the cancer vaccine resulted in increased proportions of DCs that expressed CD80 and CD86 costimulatory markers two days after the final vaccination in both popliteal and inguinal lymph nodes compared to untreated controls and monotherapy controls (Figure 4b-e). The combination treatment only minimally benefited DC maturation status in spleens, and no changes to maturation status were observed for DCs in tumors (Figure 4f-i). These results demonstrate that

combination of propranolol and a peptide cancer vaccine enhanced DC maturation at lymph nodes proximal to the vaccine injection site.

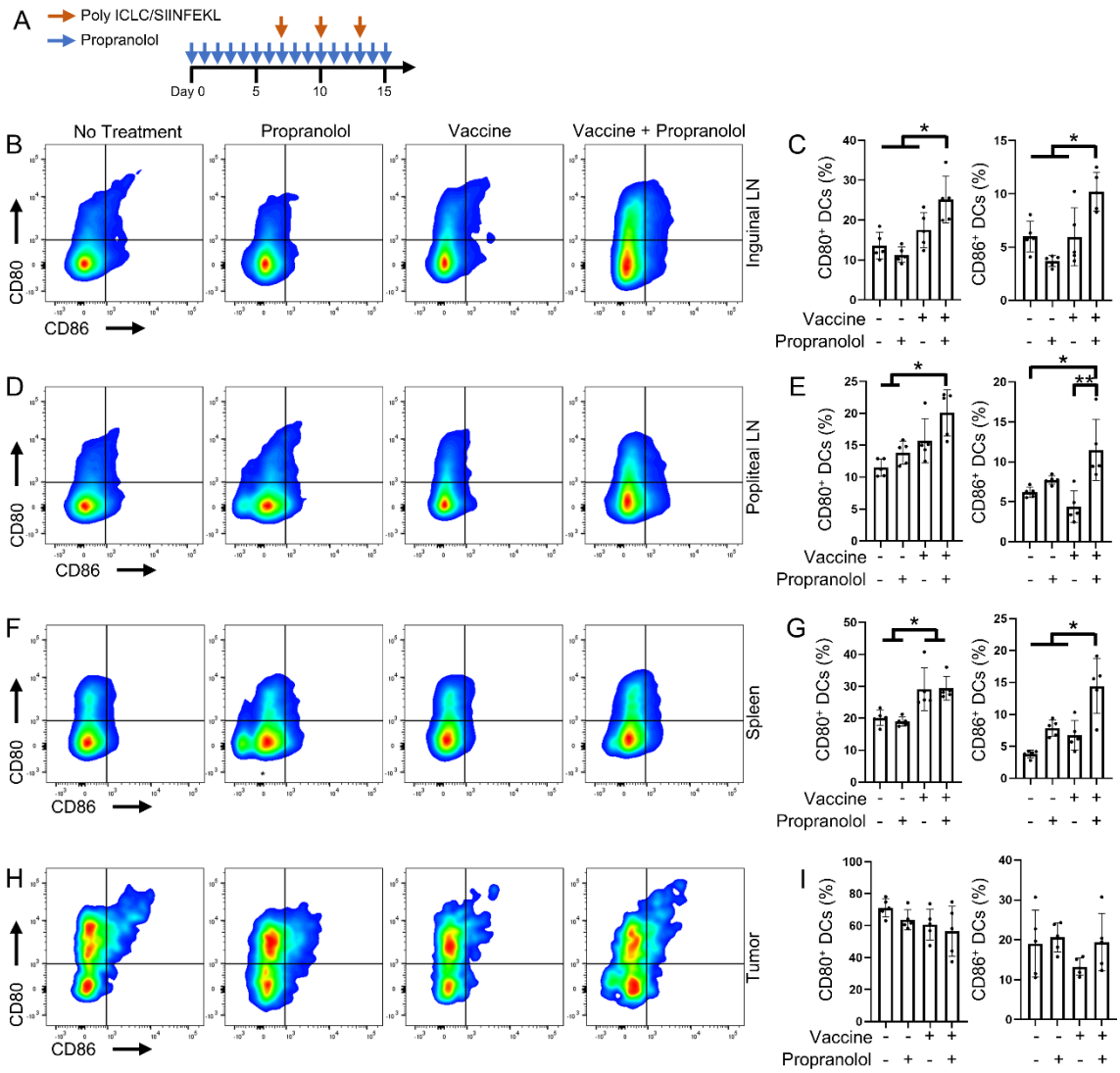

Figure 4. Propranolol enhances DC maturation following vaccination: A) C57BL/6J mice were subcutaneously inoculated with B16-OVA on day 0, given daily IP propranolol injections, and given foot pad injections of the poly ICLC/SIINFEKL vaccine according to the schematic. Mice were sacrificed on day 15 and lymph nodes, spleens, and tumors were isolated from each mouse and processed into single cell

suspensions. CD80 and CD86 surface expression on DCs in B) inguinal lymph nodes, D) popliteal lymph nodes, F) spleen, and H) tumor tissues are shown on the left, and C, E, G, I) quantification of their respective percentage positive CD80 or CD86 are shown on the right. n = 5 mice/group, and ANOVA followed by Tukey HSD post hoc tests were performed.

Propranolol favorably alters immune cell populations in size-matched B16-OVA tumors following vaccination

Since we found that sympathetic signaling affects the maturation of lymph node DCs, we aimed to evaluate how propranolol impacts immune cell populations in growing B16-OVA tumors. Tumor size can introduce a confounding variable when analyzing intratumor immune cells, so we examined immune cell populations in size-matched B16-OVA tumors by inoculating B16-OVA cells in the combination group 3 days prior (day -3) to the propranolol and no treatment groups and by inoculating B16-OVA cells in the vaccine alone group 1 days prior (day -1) to the propranolol and no treatment groups. Mice were vaccinated on days 4, 7, and 10 and given propranolol daily as shown in the Figure 5a schematic. All mice were sacrificed when tumor sizes reached approximately 1200 mm^3, and intratumor immune cell populations were analyzed via cytometry by time of flight (CyTOF). We found that both the vaccine alone group and the combination propranolol plus vaccine group experienced an increase in total intratumor $CD8^+$ T cells among $CD45^+$ cells as well as increases in the proportion of $CD8^+$ effector memory T cells (T_{EM}) and PD-1^+CD8^+ T cells among $CD45^+$ cells (Figure 5b, c). However, the combination of propranolol plus vaccine group experienced

significantly greater increases in total $CD8^+$ T cells, $CD8^+$ T_{EM} cells, and PD-1^+CD8^+ T cells compared to vaccination alone with approximately 4.8-fold, 13-fold, and 5.8-fold increases over no treatment, respectively (Figure 5c). Vaccination alone only resulted in approximately 2.3-fold, 4.6-fold, and 2.5-fold increases in $CD8^+$ T cells, $CD8^+$ T_{EM} cells, and PD-1^+CD8^+ T cells over no treatment, respectively (Figure 5c). Combination of propranolol plus vaccine also resulted in a significant 2.4-fold increase in total intratumor $CD4^+$ T cells among $CD45^+$ cells, whereas vaccination alone did not result in an increase in $CD4^+$ T cell number (Figure 5c). Additionally, propranolol alone resulted in a significant decrease in the proportion of $Foxp3^+CD4^+$ T cells compared to each other group, but this change to $CD4^+$ T cell Foxp3 expression was not observed in the combination group (Figure 5e). It has been previously reported that loss of sympathetic signaling will reduce expression of the immune checkpoint molecules PD-1 and CTLA-4 on intratumor $CD8^+$ and $CD4^+$ T cells [24]. However, we did not observe decreased expression of either of these molecules in either the propranolol alone group or the combination group (Figure 5d, e).

Combination of propranolol plus vaccine also resulted in significant changes to immunosuppressive myeloid cell populations. The combination group exhibited significant decreases in the proportions of total polymorphonuclear MDSCs (PMN-MDSCs) and PD-$L1^+$ PMN-MDSCs among $CD45^+$ cells compared to the no treatment group (Figure 5b, f). Both propranolol alone and propranolol plus vaccine groups experienced a decrease in the percentage of PD-$L1^+$ PMN-MDSCs among total PMN-MDSCs compared to the no treatment group (Figure 5g). On the other hand, vaccination

alone exhibited the same percentage of PD-L1$^+$ PMN-MDSCs among total PMN-MDSCs as the no treatment group and was significantly higher than the combination group (Figure 5g). While the combination group only experienced a nonsignificant decrease in monocytic MDSCs (M-MDSCs) among CD45$^+$ cells, it did exhibit significantly decreased PD-L1$^+$ M-MDSCs among CD45$^+$ cells compared to the no treatment group (Figure 5b, f). Propranolol treated mice also experienced a significant decrease in PD-L1$^+$ M-MDSCs among CD45$^+$ cells compared to the no treatment group (Figure 5b, f). Both propranolol and the combination groups also experienced significant decreases in the percentage of PD-L1$^+$ M-MDSCs among total M-MDSCs compared to the no treatment group, and the percentage of PD-L1$^+$ M-MDSCs in the combination group was significantly lower than both the vaccine alone and propranolol alone groups (Figure 5h). Taken together, these findings suggest that propranolol alone and the combination of propranolol and a cancer vaccine can minimize PD-L1$^+$ MDSCs.

Combination of propranolol and vaccine also affected the MDSC enzymes inducible nitric oxide synthase (NOS2) and arginase-I (Arg-I), which are both associated with tumor-promoting and immunosuppressive functions [74]. The combination group experienced a significant decrease in the percentage of PMN-MDSCs expressing NOS2 compared to the no treatment group as well as a significant decrease in Arg-I$^+$ PMN-MDSCs compared to no treatment and vaccine alone groups (Figure 5g). Interestingly, propranolol alone, vaccine alone, and the combination group each exhibited reduced Arg-I$^+$ M-MDSCs compared to the no treatment group (Figure 5h). Lastly, the combination propranolol plus vaccine group exhibited significantly reduced TAMs

compared to the vaccine group (Figure 5b, f). These results show that combination of propranolol plus a Poly ICLC/peptide cancer vaccine improves intratumor immune cell populations by increasing the proportion of effector $CD8^+$ T cells and decreasing regulatory cell types including MDSCs and TAMs.

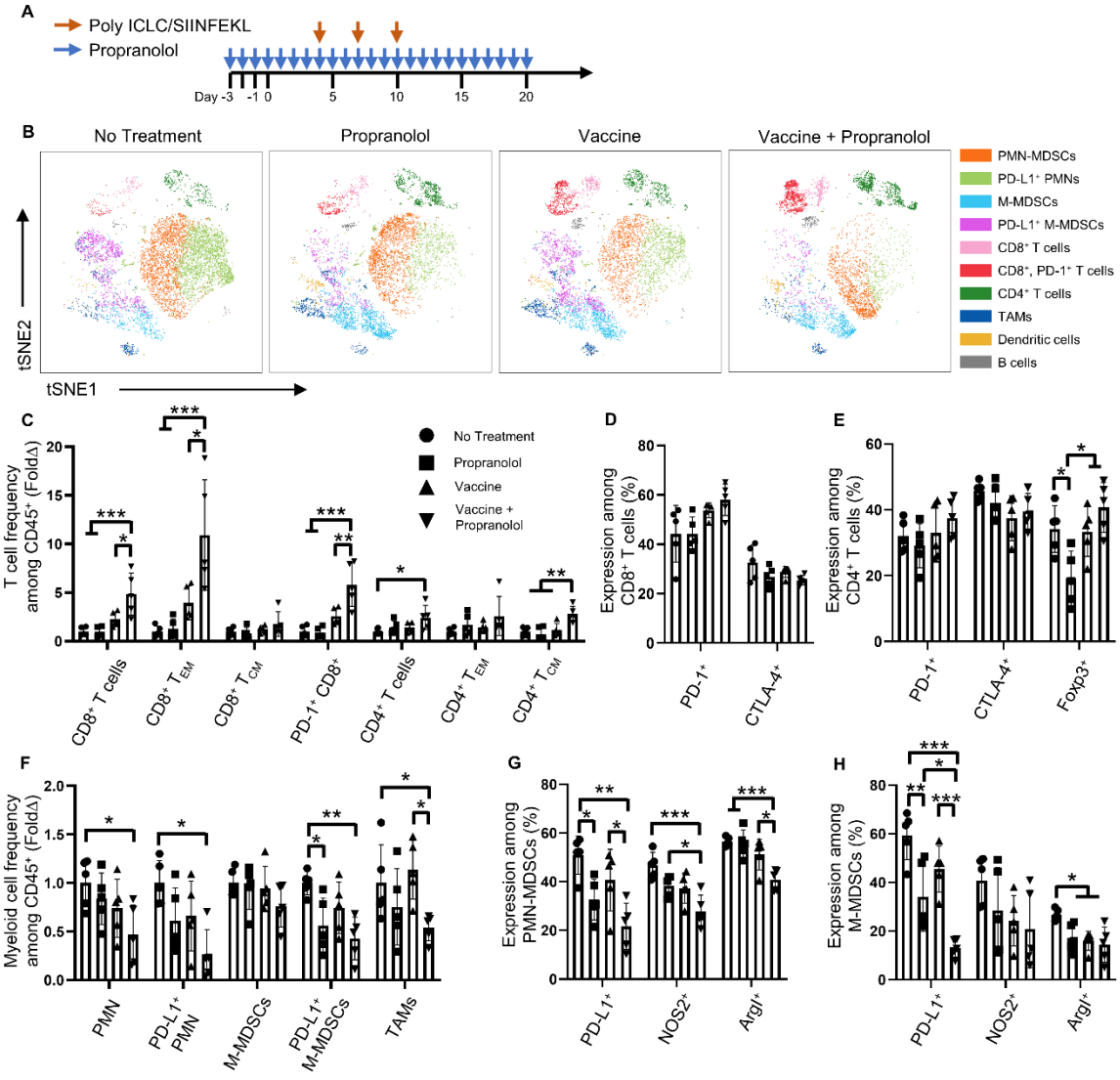

Figure 5. Propranolol favorably alters immune cell populations in size-matched B16-OVA tumors following vaccination: C57BL/6J mice were subcutaneously inoculated with B16-OVA on days -3, -1, or 0, given daily IP propranolol injections, and given foot

pad injections of the poly ICLC/SIINFEKL vaccine according to the schematic presented in figure 6A. The vaccine + propranolol combination group were inoculated with B16-OVA on day -3, the vaccine group was inoculated on day -1, and the no treatment and propranolol groups were inoculated on day 0. Once each group reached approximately 1200 mm^3 tumor volumes, mice were sacrificed and tumors were dissected and digested into single cells suspensions, which were then analyzed by CyTOF. B) Representative t-SNE plots from each treatment group gated on $CD45^+$ cells with color-coded cell populations overlaid are shown. C) Fold change over untreated control group of indicated T cell population frequencies among total $CD45^+$ cells were calculated. Percentage of D) $CD8^+$ T cells and E) $CD4^+$ T cells that expressed PD-1, CTLA-4, or Foxp3 are shown. F) Fold change over untreated control group of indicated myeloid cell population frequencies among total $CD45^+$ cells were calculated. Percentage of G) PMN-MDSCs and H) M-MDSCs that expressed PD-L1, NOS2, and ArgI are shown. n = 5 mice/group, and ANOVA followed by Tukey HSD post hoc tests were performed.

Propranolol improves therapeutic vaccine treatment of B16-OVA melanoma

Based the observed benefits to DC maturation and intratumor immune cells in propranolol plus vaccine treated mice, we hypothesized that this combination would improve cancer vaccine treatment of melanoma in mice. To test this combination, we performed another therapeutic vaccine study according to the schematic in Figure 6a.

The propranolol plus vaccine combination group experienced dramatically reduced tumor volumes (approximately 300 mm^3) by day 20 compared to the untreated

control group (approximately 1700 mm^3) as well as compared to the monotherapy treatment groups (Figure 6b). The vaccine monotherapy group had slightly reduced tumor volumes (approximately 1200 mm^3) compared to untreated mice by day 20, but this difference did not reach statistical significance. The propranolol monotherapy group did not differ in tumor growth compared to the untreated control group. In addition, we isolated splenocyte samples from these groups to test for systemic immune responses to the vaccine peptide SIINFEKL. After incubating splenocytes from each group with SIINFEKL peptide on IFN-γ coated ELISPOT plates for 48 hours, we found that combination of propranolol and the vaccine led to an approximately 2.5-fold increase in IFN-γ producing splenocytes compared to vaccine monotherapy (Figure 6c). These results show that combination of propranolol with a peptide cancer vaccine improved treatment of melanoma in mice as well as improved systemic IFN-γ production.

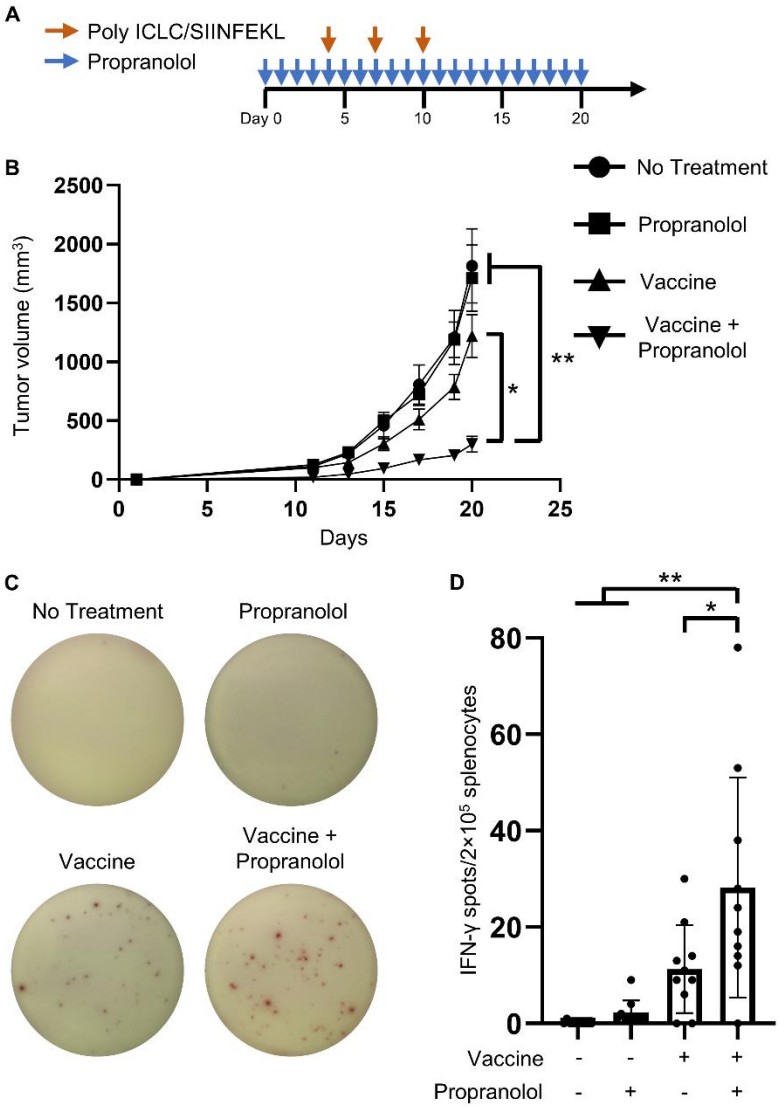

Figure 6. Propranolol improves therapeutic vaccine treatment of B16-OVA melanoma:

A) C57BL/6J mice were subcutaneously inoculated with B16-OVA on day 0, given daily IP propranolol injections starting day zero, and given foot pad injections of the Poly ICLC/SIINFEKL vaccine on days 4, 7, and 10 according to their treatment groups. B) Tumor volumes were calculated starting day 11 and repeated every 2 days until each group was sacrificed on day 20. C) Spleenocytes were harvested from each mouse on

day 20 and incubated with 10 μg/ml SIINFEKL peptide on IFN-γ antibody-coated ELISpot plates for 48 hours. After color development, number of spots per well were counted with a digital ELISPOT plate reader. n = 10 mice/group, and ANOVA followed by Tukey HSD post hoc tests were performed on tumor volumes at day 20.

Discussion

In this study, we report the novel finding that $CD115^+$ moMΦ in BMDC cultures are responsible for the observed changes to cytokine production following norepinephrine treatment, whereas $CD115^-$ DCs do not express surface β_2AR and are unresponsive to norepinephrine treatment. In addition, $CD115^+$ moMΦ experience reduced ability to stimulate $CD8^+$ T cell proliferation after norepinephrine treatment, whereas $CD115^-$ DC stimulation of $CD8^+$ T cell proliferation is unimpaired by norepinephrine. This relationship appears to hold true *in vivo* since we demonstrated that DCs in mouse lymph nodes and spleens do not express surface β_2AR, but macrophages and moDCs in these tissues do express β_2AR on their surfaces. GM-CSF grown BMDC cultures have been previously used to demonstrate that β_2AR signaling impairs DC production of IL-12p70 and subsequent priming of T_H1 cells [61] [63] [75]. However, these studies did not account for heterogeneity within $CD11c^+MHCII^+$ BMDC cells, which is known to be comprised of at least two distinct cell populations based on intermediate or high expression of MHCII, cell ontogeny, and macrophage versus DC gene expression patterns [59]. We found that CD115 alone is an adequate marker to separate DCs and moMΦ in BMDC cultures, evident by unique cell morphology, expression of DC markers, and ability to stimulate $CD8^+$ T cell proliferation. We then

demonstrated that β_2AR signaling does not directly impact DCs as previously reported, but instead directly affects β_2ARs on moMΦ. Importantly, this *in vitro* observation correlates with our finding that mouse lymph node and spleen cDCs lack surface β_2ARs, which further supports the claim that MHCII^{hi}CD115^{-} BMDC more closely resemble mouse cDCs than MHCII^{int}CD115^{+} BMDC, which instead are similar to moMΦ [59]. cDCs receive much attention as mediators of adaptive immunity, but circulating monocytes and peripheral moMΦ can migrate to lymph nodes and adopt APC characteristics under inflammatory conditions to modulate T cell responses [52] [53]. These MCs contribute to T cell priming and exhibit distinct and nonredundant functionality compared to DCs [52] [53] [55]. Our results indicate that moMΦ possess a unique role compared to cDCs as key mediators of SNS regulation of the APC immune compartment.

We additionally explored the impact of sympathetic signaling on cancer vaccine activity by evaluating DC function, intratumor immune cells, and tumor growth in melanoma-bearing mice that were treated with a combination of the non-specific β-blocker propranolol and a peptide cancer vaccine. While it is commonly acknowledged that altered APC function could contribute to sympathetic regulation of tumor immunity, SNS regulation of APCs remain underexamined in studies investigating the impact of sympathetic signaling on cancer immunotherapy. Studies into SNS regulation of tumor immunity have also typically been focused on a single immune cell type, so a comprehensive analysis of changes to intratumor immune cell types is lacking. In the studies presented here, we demonstrate that combination of propranolol and a cancer

vaccine improved DC maturation in lymph nodes near the vaccination site evident by increased expression of CD80 and CD86 costimulatory markers. This finding is consistent with previous reports that increased SNS tone will impair DC maturation and that blockade of SNS signaling will improve APC function and subsequent T cell priming [56] [76] [50]. Despite our finding that mouse DCs lack β_2AR, propranolol improved DC maturation following vaccination, possibly by altering the local inflammatory milieu.

In size matched B16-OVA tumors, we found that combination of propranolol with a peptide vaccine increased the proportion of $CD8^+$ T cells among $CD45^+$ cells compared to vaccination alone. Additionally, the combination group exhibited dramatically higher amounts of activated $PD\text{-}1^+CD8^+$ T cells and $CD8^+$ T_{EM} cells compared to vaccination alone. Furthermore, propranolol alone resulted in significantly reduced proportions of $Foxp3^+CD4^+$ T cells. However, this decrease was not observed in the combination group. This change in $Foxp3^+$ expression is consistent with a previous study showing that denervation of sympathetic nerves at breast tumors resulted in decreased expression of Foxp3 in $CD4^+$ T cells [24]. This study also reported decreased PD-1 and CTLA-4 expression on both $CD8^+$ and $CD4^+$ T cells [24], but we did not observe a decrease in PD-1 or CTLA-4 expression on either $CD8^+$ or $CD4^+$ T cells in the propranolol or combination groups in our study. This discrepancy in observed immune checkpoint molecule expression might be due to the differences inherent to incomplete inhibition of SNS signaling by propranolol treatment in our study and the impact of complete denervation of sympathetic nerves in the previous study [24].

In addition to the observed changes to T cells, the combination of propranolol and a cancer vaccine favorably altered several myeloid cell populations. The combination group had significantly reduced total PMN-MDSCs among $CD45^+$ cells compared to no treatment as well as dramatically reduced PD-$L1^+$ PMN-MDSCs. Similarly, the combination of propranolol plus vaccine resulted in significantly reduced PD-$L1^+$ M-MDSCs compared to no treatment. We found that propranolol alone significantly decreased the percentage of PMN-MDSCs and M-MDSCs that express PD-L1, which potentially explains the dramatic reduction in PD-$L1^+$ MDSCs observed in the combination group. These observed reductions in PD-$L1^+$ MDSCs are consistent with a previous study that reported that β_2AR signaling greatly supports MDSC survival and immunosuppressive functions [10]. It was reported that β_2AR signaling in MDSCs was associated with increased PD-L1 expression, increased STAT3 phosphorylation, and decreased apoptosis gene signatures [10]. However, it is unclear how β_2AR signaling mediates STAT3 phosphorylation, which regulates many immunosuppressive functions in MDSCs [77]. Based on our findings, β_2AR-mediated increases in IL-10 could potentially explain increased STAT3 phosphorylation and associated immunosuppressive functions in MDSCs, but further studies into this relationship are needed. In addition, the combination group exhibited significantly reduced TAMs compared to the vaccine group. This finding is consistent with two previous studies that found that βAR signaling contributes to TAM infiltration into tumors, M2 polarization, and cancer progression [29] [11]. These animal model studies are supported by *in vitro* findings that norepinephrine polarizes macrophages towards an M2, protumorigenic

phenotype [45]. Despite these connections between βAR signaling and M2 polarization, we did not observe a change in the proportion of M2 to M1 TAMs in either the propranolol or combination groups.

Another study that combined propranolol and a cancer vaccine was recently published and similarly showed a dramatic improvement in anti-cancer efficacy [49]. The authors demonstrated that naïve $CD8^+$ T cells are responsive to β_2AR signaling but limited their evaluation of DC function to *in vitro* analyses and did not evaluate changes to the intratumor myeloid environment. In contrast, we show that the combination of propranolol and a vaccine resulted in improved DC maturation in lymph nodes, which likely improves naïve T cell priming. In addition, the combination treatment in our study dramatically minimized immune regulatory elements through changes to MDSC and TAM populations. Thus, we present novel findings into SNS modulation of the myeloid cell compartment in lymph nodes and the tumor environment that impair cancer vaccine activity. We additionally provide a more comprehensive evaluation of how propranolol will impact multiple immune cell types following vaccination.

In conclusion, our results show that SNS signaling directly impacts moMΦ rather than DCs and that combination of a β-blocker with a cancer vaccine dramatically improves antitumor efficacy in the treatment of melanoma in mice. This combination treatment resulted in improved DC expression of costimulatory molecules at lymph nodes proximal to the vaccination site, increased intratumor total and effector $CD8^+$ T cells, and minimized immunoregulatory MDSCs and TAMs in the tumor microenvironment. Based on these benefits, our study provides strong support for the

combination of β-blockers with cancer vaccines in a clinical setting. β-blockers such as propranolol are widely prescribed and rarely contraindicated, so they are poised to be rapidly repurposed for use in combination with cancer immunotherapeutics. Our study also demonstrates the need to delineate myeloid subpopulations in BMDC cultures when studying DC biology.

CHAPTER III

PROJECT 2: NANO ENCAPSULATED NOVEL COMPOUND SA-10 WITH THERAPEUTIC ACTIVITY IN BOTH ACUTE AND CHRONIC MURINE HINDLIMB ISCHEMIA MODELS[*]

Introduction and Literature Review

Peripheral Ischemia Disease burden

Peripheral arterial disease (PAD) is a disease of the lower extremities where one or several peripheral arteries are narrowed or blocked. The annual cost for PAD-related health care in the US is $10-$20 billion dollars [78]. According to American Heart Association (AHA) statistics, at least 200 million people worldwide suffer from PAD [79] [80]. In the US, 8.5 million PAD patients (12% of American adults) are ages 40 or older, and about 20% of PAD patients are over 70 years of age [78] [81]. Progression of PAD is critical limb ischemia (CLI), which requires either endovascular revascularization or surgery to restore blood perfusion. Endovascular revascularization includes balloon dilation (angioplasty), cutting balloons, drug-coated balloons, covered stents, drug-eluting stents, and atherectomy. The surgical bypass is usually performed on femoral and proximal popliteal arteries where the issues of stenosis and occlusion commonly happen [81], and autologous vein bypass transplantation is considered first line therapy [78] [82]. Nevertheless, the intervention often causes thrombosis and

[*] Reprinted with permission from "Nano encapsulated novel compound SA-10 with therapeutic activity in both acute and chronic murine hindlimb ischemia models" by Louis Hinkle, Duong Le, Tam Nguyen, Vy Tran, Charles E. Amankwa, Courtney Weston, Haifa Shen, Kytai Nguyen, Maham Rahimi, Suchismita Acharya. 2021. Nanomedicine: Nanotechnology, Biology and Medicine, 35(102400), 1-11, Copyright 2021 by Elsevier Inc.

restenosis, and approximately 20-30% of PAD patients with CLI are not suitable candidates to undergo either surgery or endovascular revascularization. Recently, enhancing angiogenesis to treat PAD attracted more attention since it avoids invasive surgical intervention [83].

Acute limb ischemia has an incidence of 1.5 cases per 10,000 persons per year and is associated with high rates of death and complication [84]. Acute limb ischemia results from a sudden decrease in limb perfusion that threatens limb viability and requires immediate diagnosis and revascularization. It can be caused by cardiogenic thromboembolism, in situ thrombosis, and vascular injury. Reperfusion is necessary to prevent tissue loss, but paradoxically also induces further tissue damage after return of blood flow. Ischemia/reperfusion (I/R) injury can result in tissue compartment swelling, endothelial dysfunction, and sterile inflammation. A devastating complication of reperfusion injury is multiorgan dysfunction syndrome (MODS). The inflammatory response to I/R injury in skeletal muscle can be so intense that distant organs are affected. The lung is the most commonly damaged organ in MODS, and it is characterized by progressive hypoxemia, pulmonary edema, and accumulation of neutrophil-rich alveolar fluid [85] [86]. The molecular mechanisms that contribute to endothelial dysfunction and inflammation in I/R injury is multifactorial, but the sudden return of oxygen and generation of ROS appears to be a driving contributor.

Molecular mechanisms underlying I/R injury

NO dysregulation has been strongly implicated in the underlying mechanisms of ischemic injury due to its role in reducing endothelial damage and ROS generation. NO

is synthesized in endothelial cells from L-arginine by NO synthase (NOS) and contributes to vasodilation tone, local cell growth, and control of platelet activation [87]. NO production by endothelial cells is regulated at a basal level by the constitutively expressed endothelial NOS (eNOS). During periods of inflammation, an inducible form of NOS (iNOS) produces large surges of NO [88]. Manipulation of NO production during I/R injury has been shown to alter local and distant tissue damage such that low doses of NO were protective, but high doses proved to be cytotoxic [89]. Consistent with this, overexpression of eNOS, which produces NO in picomolar amounts, led to reduced superoxide, reduced micro-vascular leakage, and reduced expression of intercellular adhesion molecules on endothelial cells [89]. iNOS deficient mice also protect against I/R injury in skeletal muscle, which supports the claim that high amounts of NO can lead to cytotoxic effects [90]. Based on these findings, controlled, low dose delivery of NO would attenuate I/R injury.

ROS generation also contributes to tissue damage and inflammation following I/R injury. During periods of ischemia, ATP metabolism into uric acid is interrupted by the presence of xanthine oxidase, which requires oxygen to convert hypoxanthine into xanthine and eventually uric acid. Once blood flow returns during reperfusion, xanthine oxidase is able to convert the accumulated hypoxanthine into xanthine, but produces superoxide as a byproduct [91]. The role of xanthine oxidase in I/R injury is supported by studies showing that xanthine oxidase inhibition minimizes remote organ damage following I/R injury [91]. There is an additional burst of superoxide from mitochondria following reperfusion that is unrelated to cytosolic xanthine oxidase [92]. The collective

surge of superoxide can directly damage surrounding tissues, but also leads to the formation of other reactive species including hydrogen peroxide and peroxynitrite that contribute to tissue damage and inflammation [93]. Superoxide and other ROS are strongly oxidizing molecules that are toxic to cell membranes and directly activate immune cells. ROS damage cell membranes through lipid peroxidation, and this can be detected by a marked increase in lipid peroxidation products in plasma following I/R injury [94]. Necrotic cell products stimulate the release of inflammatory cytokines such as IL-6, which activate endothelial cells to initiate leukocyte adhesion and promote leukocyte infiltration. Neutrophil activation strongly contributes to endothelial cell dysfunction and distant organ involvement since they produce superoxide and hydrogen peroxide and secrete proteases that degrade tissue basement membranes [95] [96]. Circulating activated neutrophils ultimately leads to lung damage by inducing pulmonary vascular dysfunction and permeability.

Therapeutic options to address NO and ROS during I/R injury

Current first line treatment options for peripheral ischemia, whether in the setting of acute occlusion or CLI, are limited to immediate endovascular or surgical methods of revascularization. These invasive methods alone do not address the complications of ROS generation and NO dysregulation following reperfusion [97]. Several novel approaches have emerged to address the multifactorial, molecular pathogenesis of I/R injury, including enhanced angiogenesis, ischemia conditioning, NO delivery, and limiting ROS [83] [98] [99] [100]. Therapeutic angiogenesis aims to aims to enhance the formation of new vasculature to restore circulation to ischemic tissues. VEGF is key to

the formation of new blood vessel under homeostasis, and delivery of VEGF has shown promise in the treatment of preclinical models of cardiac and peripheral ischemia [101] [102] [103]. Despite prolific success in animal models, delivery of VEGF via protein or DNA plasmid in humans has been underwhelming in the treatment of ischemia related diseases. VEGF delivery clinical trials often revealed no improvement over placebo in primary endpoints such as mobility and limb amputation [104] [105]. The minimal benefits observed in clinical studies could be due to the limitations inherent to VEGF as a monotherapy, or the possibility that VEGF receptor downregulation mediates ischemia related diseases in humans rather than low VEGF availability [106]. Other pro-angiogenic drugs being explored for treatment of ischemia-related diseases include fibroblast growth factors (FGF) 1 and 2 and Hepatocyte growth factor (HGF). Similar to VEGF, FGFs and HGF showed promising results in animal models of peripheral ischemia, but exhibited virtually no benefit over placebos for primary endpoints in phase III clinical trials for FGF and minimal benefits for primary endpoints for HGF in phase II and III clinical trials [107] [108] [109]. Based on these clinical trials, pro-angiogenic factors as monotherapies are likely insufficient to address reperfusion injury.

Another innovative method being explored for reperfusion injury treatment is ischemia conditioning. Conditioning refers to transient ischemia episodes either prior to or following a larger ischemia event that ultimately minimizes tissue damage caused by the larger ischemia event. Clinic evidence for possible therapeutic benefits of ischemia conditioning can be illustrated by patients who experience transient ischemia attacks (TIA) prior to cerebral infarction. These patients exhibit improved motor function and

reduced infarct size compared to patients who experience cerebral infarction without prior TIA [110]. Preconditioning has shown similar protective benefits in other organs that experience ischemia and infarction. Short periods of ischemia prior to 40 minute coronary occlusion limited myocardial infarct sizes in animals [111], and ischemic preconditioning of livers confers tissue protection and improves transplant viability [112]. Therapeutic ischemia preconditioning is only applicable in patients with predictable episodes of ischemia, so ischemia postconditioning has been explored for acute ischemia events that threaten myocardial tissue and limb viability. Ischemia postconditioning of myocardial tissues can be achieved in humans by pharmacological or angioplasty methods and has shown great clinical promise in improving surrogate outcomes including myocardial biomarker release, infarct size, and ST-segment regression [113]. However, the first clinical trial assessing primary clinical outcomes of total mortality and hospitalization for heart failure revealed no benefit with use of cyclosporin as a pharmacological means of ischemia postconditioning [114]. Use of ischemia postconditioning for acute limb ischemia treatment has not been explored in human patients to the same extent as myocardial and cerebral postconditioning, but has shown promising results in preclinical studies [115]. While the mechanisms underlying pre/postconditioning are still unclear, it appears that transient ischemia before or after larger ischemic events will minimize ROS generation and inflammation and upregulate eNOS activity [98]. While ischemia conditioning has not yet reached wide clinical application for myocardia infarction, stroke, or acute limb ischemia, preclinical and

clinical results for these methods have achieved impressive benefits as well as further validated ROS and NO as critical mediators of reperfusion injury.

As discussed above, NO dysregulation is a key mechanism underlying I/R injury such that high amounts NO production by iNOS in inflammatory settings is cytotoxic, and loss of picomolar amounts of NO by eNOS undermines endothelial health and revascularization [88] [89]. Based on the pivotal role of NO in I/R injury, delivery of NO for the treatment of I/R injury has been widely explored in animal models and has reached limited testing in human clinical trials. Delivery of NO donor agents (either inhaled NO, sodium nitroprusside, or nitroglycerin) for the treatment of myocardial infarction in human patients has shown mitigated I/R injury outcomes in several studies based on improved revascularization, improved thrombolysis in myocardial infarction scores, and/or reduced incidence of death [116] [117] [118]. Similarly, delivery of NO donors (potassium nitrate, isosorbide mononitrate, pentaerythrityl, and inhaled NO) in human limb tourniquet studies resulted in improved flow-mediated vessel dilation and reduced inflammatory markers [119] [120]. However, delivery of NO agents in humans has not yielded universally beneficial results [121] [122]. In fact, several studies utilizing NO donors following cardiopulmonary bypass or myocardial infarction reported increased adverse reactions related to hypotension that were either transient or severe enough to require vasopressor treatment [123] [116]. The limited benefit observed in some of these clinical trials might be related to the potential for NO to be harmful at high concentrations, or it could be due to the limitations of NO as a monotherapy. ROS generation has also been highly implicated in I/R injury pathogenesis, and ROS

scavenger treatment of I/R injury have shown great promise in animal models [124]. However, there has been limited application of ROS scavengers in clinical trials, and the limited number of clinical trials showed no benefit over placebo for the treatment of myocardial infarction [125] [126]. These novel strategies attempt to address the mechanisms underlying reperfusion injury, but each were unable to achieve the expected therapeutic benefits when transitioning to human clinical trials. These limitations are potentially due to the limitations of each of these treatment strategies as monotherapies.

A novel class of hybrid NO donor/ROS scavenger drugs

Delivery of therapeutic doses of NO for the treatment of skeletal muscle I/R injury has shown promising results in animal models, but its application is limited by the generation of ROS during reperfusion. When NO is delivered in a ROS-rich environment, the two will react to produce peroxynitrite, which is a strong oxidizer that further contributes to lipid peroxidation, mitochondrial dysfunction, and systemic inflammation [127] [128]. ROS surges during I/R injury and overwhelms natural antioxidants such as glutathione. For this reason, it is important to take into consideration ROS levels during I/R injury when delivering therapeutic doses of NO. Our lab has previously reported the design of a hybrid molecule 4-amino TEMPOL-H sydnonimine (SA-2) that combines a pH-responsive NO donor and superoxide dismutase (SOD) mimetic functional groups [13]. The NO donor portion of this hybrid molecule utilizes a sydnonimine ring structure, which releases NO in slightly alkaline environments ($>pH_{7.4}$) [129]. The piperidine nitroxide TEMPOL portion of the molecule is an effective antioxidant through its action as a catalytic SOD mimetic [130]. SA-2

successfully maintained physiological levels of eNOS in human umbilical vascular endothelial cells (HUVECs) under H_2O_2 oxidative stress. Additionally, SA-2 decreased the levels of ROS in HUVECs under H2O2 oxidative stress. We have also recently reported that SA-2 protects retinal ganglion cells from ischemic and reperfusion induced cell death by upregulating SOD enzyme. These *in vitro* studies suggest that combination of a NO donor and ROS scavenger could protect endothelial cells in the setting of I/R injury and that the SA-2 design is a promising candidate for treatment of animal models of skeletal muscle I/R injury. Further structure activity optimization led to a more potent hybrid compound (WO/2020/132496) SA-10 containing sulfone functional groups rather than SOD mimetic motifs. In the studies presented here, we report the superior *in vitro* cytoprotective, angiogenic, and eNOS upregulating activities of SA-10 compared with SA-2. Additionally, we show that SA-10 packaged in PLGA nanoparticles effectively minimize local and remote tissue damage in two models of murine hindlimb I/R injury.

Materials and Methods

Chemicals and reagents

Following the synthetic route developed for synthesis of compounds SA-2 in our lab and reported earlier [12], compound SA-10 was synthesized. The detail method of synthesis and spectroscopical characterization of SA-10 is reported in the patent (WO2020132496). Human and mouse VEGF were purchased from Prospec Co. (East Brunswick NJ, USA). Compound GW505156 was purchased from Matrix Scientific (Columbia, SC, USA).

Fabrication and characterization of SA-10 NPs

SA-10 loaded PLGA NPs were prepared using the standard single emulsion technique developed in our laboratory [131] [132] [133]. In brief, 10 mg of SA-10 was dissolved 100 µL DMSO and then transferred to 3 ml of chloroform containing 90 mg of PLGA to form an oil phase. This solution was then added dropwise into 20 ml of 5% PVA solution (water phase) followed by sonication at 40W for 10 minutes to form the SA-10 loaded NPs. The emulsion was stirred overnight to completely evaporate the organic solvent. Next, the NPs were pelleted by ultracentrifugation at 25,000 rpm for 30 minutes followed by washing twice with DI water. Finally, the NP pellet was dissolved in DI water and lyophilized to obtain a powder form.

For SA-10 characterization, standard concentrations of SA-10 in DI water were prepared. The solutions were determined absorbent at a wavelength of 240 nm. At 240 nm, a linear fit was obtained to calculate loading efficiency and drug content of SA-10 NPs. For the drug release study, four separate solutions at 5 mg/ml of SA-10 NPs in PBS (pH 7.4) were placed in a dialysis bag with MWCO 3.5-5 kDa (Spectrum, Catalog 131192), submerged in 20 ml PBS 1X pH 7.4 (so-called dialysate) and incubated at 37oC over a time range. At each time point, 1 ml of dialysate solution was pooled and replaced with the same volume of fresh PBS. Each sampling solution was then read for its absorbance value and the amount of released SA-10 was quantified against the SA-10 standard curve. Consequently, a cumulative release profile of SA-10 over time was plotted.

Doses and treatment groups

For in vitro comparison studies, compounds SA-2 and SA-10 were sterilized and dissolved in fresh media prior to use. Except for the cell protection study where 400 µM H2O2 was used, all other in vitro studies used 200 µM H2O2 to avoid excess cell death. All compounds were dissolved in low serum media (basal media with 0.2% FBS). 'No treatment' group had cells exposed to H2O2 only without any treatment while cells exposed to H2O2 and treated with VEGF served as a positive control group.

Cell protection study

HUVECs were seeded at the confluent density overnight on a 96 well plate. Cells were stressed with 400 µM H2O2 and treated with different groups for 24 hours including VEGF, SA-2, GW501516, and SA-10. Cell viability was measured using MTS assays.

Cell proliferation study

Cells were seeded at 10,000 cells/cm^2 and allowed to grow for several days. Stresses (200 µM H_2O_2) and SA-10 compound at concentrations of 0.5 µM and 5 µM were refreshed every 24 hours. Cell number were quantified at day 4 using DNA assays and calculated against the standard curve of DNA, which is converted to the correlated cell number.

Cell migration study

Transwell chemotaxis migration studies were conducted to study the effects of SA-2 and SA-10 treatment on the migration of endothelial cells under oxidative stress conditions as previously described by our group [13].

In vitro angiogenesis studies

Cultrex reduced growth factor basement membrane extracted gel (Cat. 3433-005-01, R&D Systems, Inc.) was coated on the bottom of µ-slide angiogenesis wells (Cat. 81506, iBidi GmbH Co.). Human umbilical vein endothelial cells (HUVECs) at early passages (6^{th} passage or earlier) were then seeded on gel at a seeding density of 25,000 cells/cm^2. Next, cells were treated with treatment groups (VEGF, SA-2, SA-10, SA-10 NPs) under an oxidative stress condition (200 µM H_2O_2). After 12 hours of incubation, formation of new microtubes were visualized and captured on phase contrast microscopes. Images were then stacked and processed with an angiogenesis analyzer on ImageJ.

Animal studies

Animals were purchased from Charles River Laboratories and maintained in barrier animal facilities approved by the American Association for Accreditation of Laboratory Animal Care (AAALAC) and in accordance with current regulations and standards of the United States Department of Agriculture, Department of Health and Human Services, and National Institutes of Health. All studies related to animals, including housing, surgeries, administration of nanoparticles, fluorescent imaging, blood perfusion analysis, and treadmill running tests were conducted under the approval of UTA and Houston Methodist affiliated IACUC. Proper guidelines were followed for the animals by UTA, Houston Methodist Research Institute (HMRI), and NIH Rodent Surgery Guidelines to minimize distresses.

Two mouse hindlimb ischemic models were applied. (i) The acute I/R injury model was performed on 4-6 week old C57BL/6J female mice with a shorter treatment

regimen (3 days) of SA-10 NPs against severe local and systemic injuries. (ii) The peripheral arterial disease (PAD) model, mimicking the chronic ischemia in hindlimb tissues was performed on Balb/c mice of both sexes at 30-40 weeks old to evaluate long-term treatment (30 days) of SA-10 NPs in restoring blood perfusion and physical responses for ischemic tissues.

Acute I/R injury model

To induce I/R injury, we utilized a well-established McGivney hemorrhoidal ligator band method described earlier [134] where elastic tourniquets were applied for 4 hours and then removed to allow for blood reperfusion. Mice were further received IM injections of either saline, VEGF (10 ng/kg animal), SA-10 (0.5 mg/kg), blank NPs (64 mg/kg), or SA-10 NPs (64 mg/kg, containing 0.5 mg SA-10/kg) at 0 hours, 24 hours, and 48 hours after tourniquet removal. To maintain therapeutic doses for immediate treatment in this acute model, SA-10 NPs dose was increased 4-fold. Mice were sacrificed 72 hours post injury and gastrocnemius and lung tissues were collected for further studies.

PAD model

A mouse model of unilateral hindlimb ischemia was performed as previously described [135]. Briefly, mice were anesthetized with 2% isoflurane and subcutaneously injected SR Buprenorphine (1 mg/kg) prior an initial incision on the left hindlimb. Then, the femoral artery, proximal caudal femoral artery, and superficial caudal epigastric artery were exposed and ligated [136].

Histology and cytokine measurement

Gastrocnemius and lung samples were embedded in paraffin, sectioned, and stained with hematoxylin and eosin. Muscle damage scores and lung histopathology characteristics were provided by a pathologist from the HMRI Research Pathology Core. Leukocyte infiltration into muscle tissues was quantified using the ImageJ tracking tool on 20x field of view for stained muscles for each mouse. For cytokine analysis, gastrocnemius tissues were homogenized with an electric blade, centrifuged, and the resulting supernatant samples were collected. Enzyme-linked immunosorbent assay (ELISA) was performed to quantify IL-6 and VEGF contents with normalization to 20,000 μg sample proteins following manufacturer's instruction.

Biodistribution study

PAD mice were allowed to rest for 3 days before injecting a total of 100 μL ICG nanoparticles suspension in saline at 4 mg/ml (equivalent to 16 mg of NPs/kg of mouse) via either IM (as mentioned above) or IV (tail vein) injection. Fluorescent images of ICG NPs were taken at 3 different time points (0, 24, and 48 hours) by using Kodak in vivo imaging system. Then they were sacrificed at each time point for taking ex vivo fluorescent images of different tissues (heart, lungs, liver, kidneys, spleen, healthy and ischemic hindlimbs) and measuring fluorescent intensity (760/830 nm) of those homogenized tissues to determine the biodistribution of ICG NPs in ischemia mice. In parallel, PAD ischemia mice without receiving ICG NPs served as the control background group.

Dose response study on PAD model

The PAD model followed the unilateral hindlimb ischemia model previously reported [78]. For the pilot study, mice (n=3-5) were dosed once with either 16, 32, or 128 mg of SA-10 NPs/kg of mice (containing 0.125, 0.25, or 1.0 mg of SA-10/kg of mice, respectively) via IM injection (4 injections 25 μL each at four different sites distal to the ligation site of the femoral artery: 2 injections on the front and 2 injections on the back of the injured leg) at day 3 post-surgery.

In vivo blood perfusion and physical test

Animals under treatments were measured for blood perfusion and mobility recovery. For blood perfusion, animals were anesthetized with 1.5-2% isoflurane, and blood perfusion was measured with Laser Speckle Contrast Imaging (PeriCam PSI NR, Perimed AB) [135]. Briefly, hemoglobin in shallow vessels and capillaries responded to excitation lasers with color output. The relative blood perfusion was calculated by device software (PIMSoft), and it correlated to typical pigments. To obtain consistent and precise comparison among animals, blood perfusion indexes of each animal were obtained from a ratio of relative blood perfusion of ischemic limb to that of healthy limb on the same animal. In the mobility study, treated animals were placed in individual lanes of a mice treadmill (Cat. LE8710MTS-5 lanes. Harvard Apparatus). The treadmill was set at a 30-degree inclination. Next, the animals were then stimulated with 1.5mA electrical shocks to keep running while the treadmill increased in speed. When the animal was not running for a total of 30 seconds under stimulation, the run was terminated, and the duration was recorded. Physical recovery of animals was then

quantified as covered distance until exhaustion, which was obtained from the treadmill software.

Statistical analysis

All the experiments were performed with n=3-6 if not specified. Data were expressed as mean ± SEM. The statistical analysis was assessed using ANOVA followed by post hoc Pairwise Multiple Comparisons using Holm-Sidak method on SigmaPlot version 13.0. A significant difference was considered where P values appeared ≤ 0.05.

Results

Effects of SA-10 on endothelial cell functions under oxidative stress

We have modified our previously published molecule, SA-2, to optimize its activity as a hybrid ROS scavenger/NO donor and synthesized a new compound SA-10 (Figure 7a). First, we demonstrated that SA-10 upregulated the eNOS activity in HUVECs and found that the upregulation of eNOS is similar or slightly better than SA-2 at both 0.5 and 5µM concentrations (Figure 7b). One of the important goals behind the design of SA-10 was to increase the efficacy and duration of cytoprotection and EC proliferation activities under H_2O_2 induced oxidative stress in HUVECs. To our utmost expectation, compound SA-10 successfully increased both EC viability and cell proliferation under H_2O_2 induced oxidative stress (Figure 8a, b), and the effect lasted up to 4 days for SA-10, whereas SA-2 (0.5µM) was not effective at the 4-days' time point (Figure 8b). The results for both SA-2 and SA-10 were comparable to two standard angiogenic molecules VEGF (25ng/mL) and GW501516 (0.5µM, a selective PPAR-delta agonist). To further test if these proliferated cells are functional and can migrate

and form new tubes after treatment with different concentrations of SA-10, a 2D culture angiogenesis study was used to quantify the formation of new microtubes. Here, we found that, though the cell migration ability was similar for both SA-2 and SA-10 at 0.5 µM concentration (Figure 8c), the newly designed sulfone analog SA-10 is more efficacious in the tube formation assay (Figure 8e). Of note, increasing SA-10 concentration from 0.5 to 5 µM did not increase HUVEC proliferation, migration, or tube formation under oxidative stress, which might indicate a plateaued therapeutic effect has been achieved at the optimal concentration of 0.5 µM for SA-10 in this in vitro model.

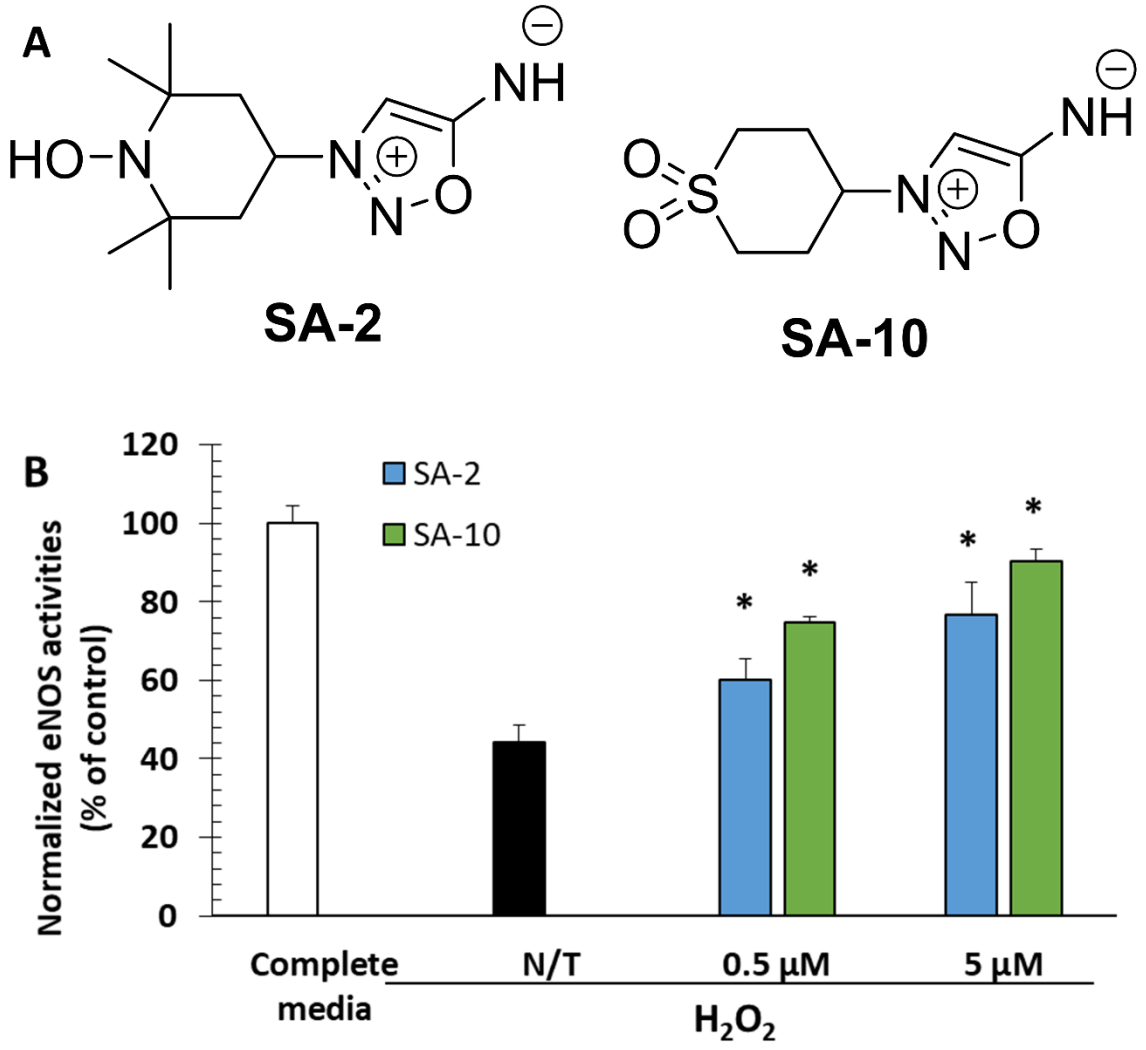

Figure 7. Effects of SA-10 on the eNOS production of ECs under stress conditions. A) Structure of the hybrid compounds SA-2 and SA-10. B) eNOS activity. HUVECs were seeded at 10,000 cells/cm^2 and treated with SA-2 and SA-10 at various concentrations. Except the positive control group where cells were exposed to complete media and no stress, all other groups had cells in low serum media with 400 µM H_2O_2; N/T groups are no treatment groups. After being treated with SA-2 or SA-10 at different concentrations under stress conditions, cells were exposed to Nitric Oxide probes of the Oxiselect^{TM}

intracellular eNOS quantification kit, and the fluorescent reading correlated to the activities of eNOS. Data is presented as mean±SD converted versus control groups. * indicates significant difference (P<0.05, n=4) compared to N/T.

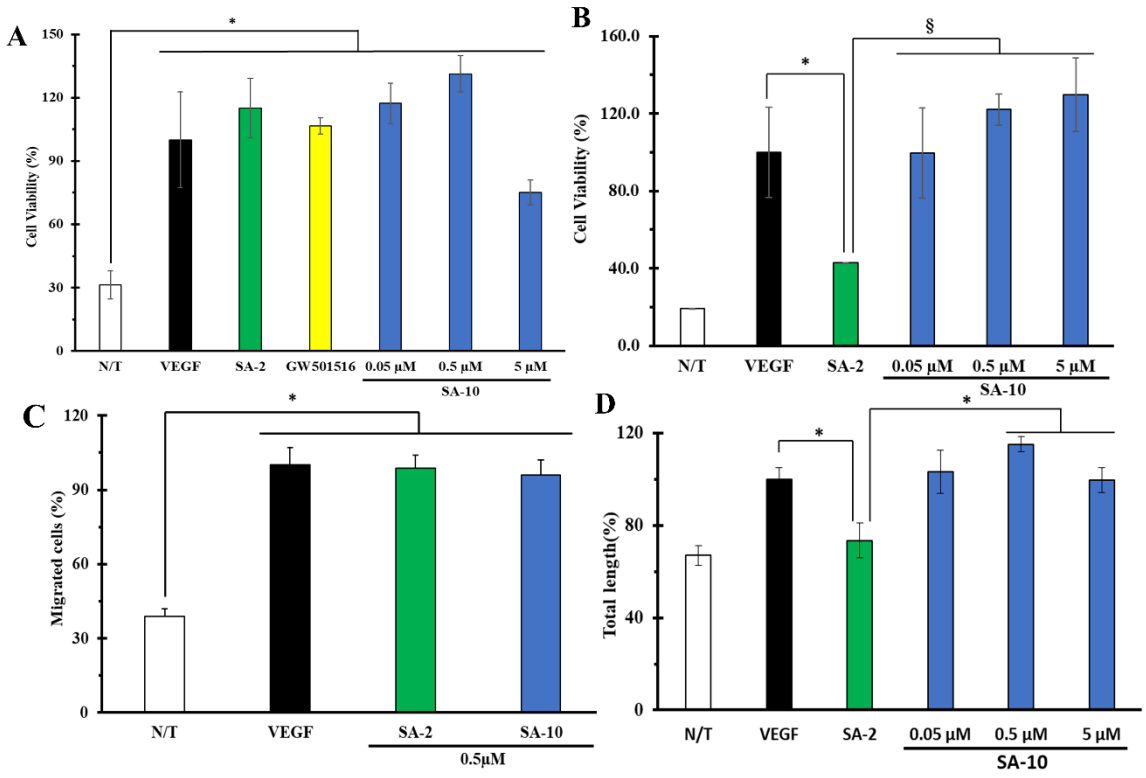

Figure 8. Effects of **SA-10** compound on HUVECs under stress conditions (H_2O_2). No treatment group (N/T: cells in 0.2% FBS with H_2O_2 only) served as negative control while VEGF (25 ng/ml), **SA-2** (0.5 µM), GW501516 (0.5 µM, PPAR δ agonist) groups served as positive controls. Treatment groups: Drug dissolved in low serum media with H_2O_2. **A)** Cell protection: cell viability analysis showed **SA-10**, **SA-2**, GW501516, and VEGF significantly protected cells under stress conditions for 1 day compared to N/T. **B)** Cell proliferation: cell growth analysis at day 4 showed **SA-10** and VEGF were significantly higher compared to **SA2** and N/T. **C)** Angiogenesis: tube formation analysis of HUVECs

on Matrigel under stress conditions at 12 hours by an angiogenesis analyzer on ImageJ. **D)** Cell migration: the number of migrated cells at 12 hours through 8μm-pore membrane were counted by a Cell counter on ImageJ. Data represented as Mean±SEM. § and * indicated significant differences where $P<0.01$ and 0.05, respectively.

Effects of SA-10-NPs on endothelial cell functions under oxidative stress

Based on the potent EC viability and angiogenic profiles in vitro, compound SA-10 was selected for the formulation optimization desired for our *in vivo* studies. We previously found that the SA-2 hybrid molecule quickly hydrolyzes in physiological, aqueous environments, and an effective sustained release of SA-2 could be achieved by packaging it in a PLGA nanoparticle carrier [13]. To ensure that SA-10 is effective over a long period of time *in vivo,* we decided to encapsulate the SA-10 molecule in PLGA nanoparticles (SA-10 NPs). The average sizes of SA-10 NPs are around 178±33nm measured by NanoBrook 90Plus PALS via dynamic light scattering (DLS) technique. Morphology of spherical SA-10 NPs were also observed under transmission electron microscopy (TEM) (Figure 9a). SA-10 NPs exhibited an initial burst release of 20% SA-10 followed by a sustained release of 60-80% over 5 days (Figure 9b) in PBS at a pH of 7.4. When tested in HUVECs under H_2O_2 induced oxidative stress condition, SA-10 NPs provided significant cell migration activity, and the effect was consistent over the range of concentrations as shown in Figure 9c.

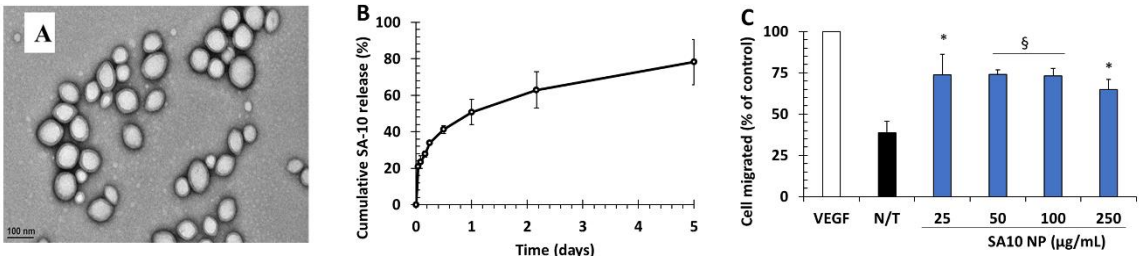

Figure 9. Effects of SA-10 NPs on HUVECs. A) TEM image of SA-10 NPs. B) Release profile of SA-10 NPs over 5 days. C) Transwell chemotaxis migration study of HUVECs under stress conditions. HUVECs were exposed to 200 µM H_2O_2 in low serum media and treated with various concentrations of SA-10 NPs and VEGF for 24 hours. Migrated cells were fixed and stained with crystal violet before being counted with ImageJ software. N/T: Cells in 0.2% FBS with H_2O_2 200 µM. VEGF served as a positive control. Data represented as Mean±SD. § and * indicated significant differences where $P<0.01$ and 0.05, respectively.

Biodistribution of ICG loaded PLGA nanoparticles

Indocyanine green (ICG) NPs, fabricated by a standard single emulsion method similar to synthesis of SA-10 NPs were used to evaluate the *in vivo* distribution and accumulation of PLGA nanoparticles after injection. We found that IM injection resulted in greater retention of nanoparticles in the injured hindlimb muscle 2 days after injection compared to IV injection (Figure 10). Additionally, IM injection showed less accumulation in kidneys compared to IV injection. Therefore, IM injection was selected for the subsequent in vivo studies for our designed NPs.

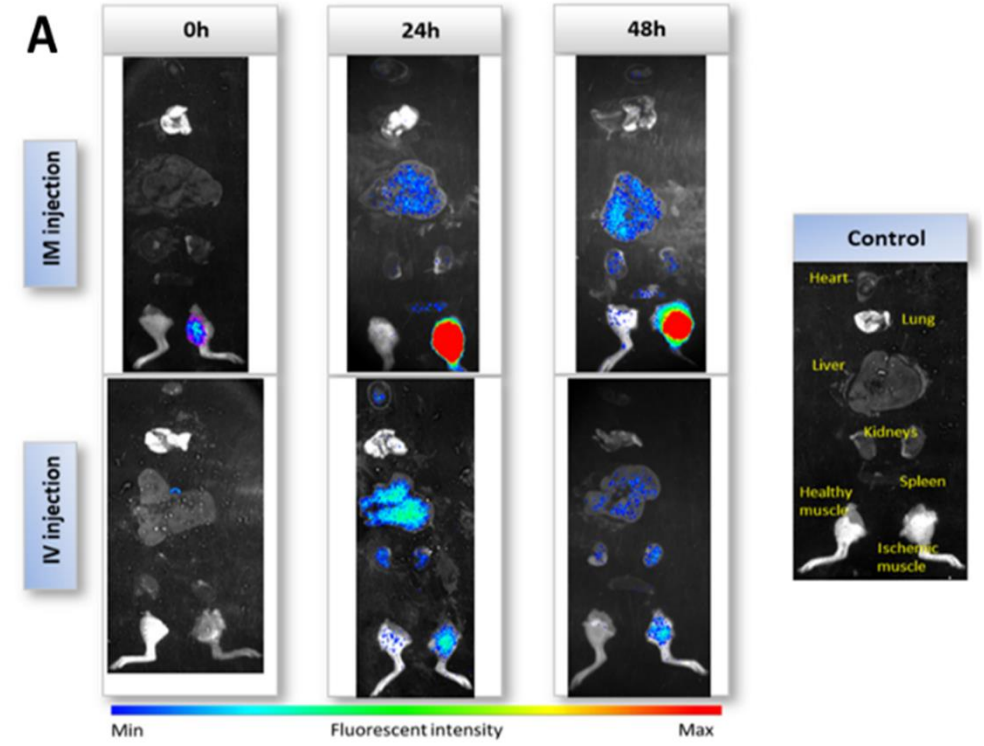
A
0h
24h
48h
IM injection
IV injection
Control
Heart
Lung
Liver
Kidneys
Spleen
Healthy muscle
Ischemic muscle
Min
Fluorescent intensity
Max

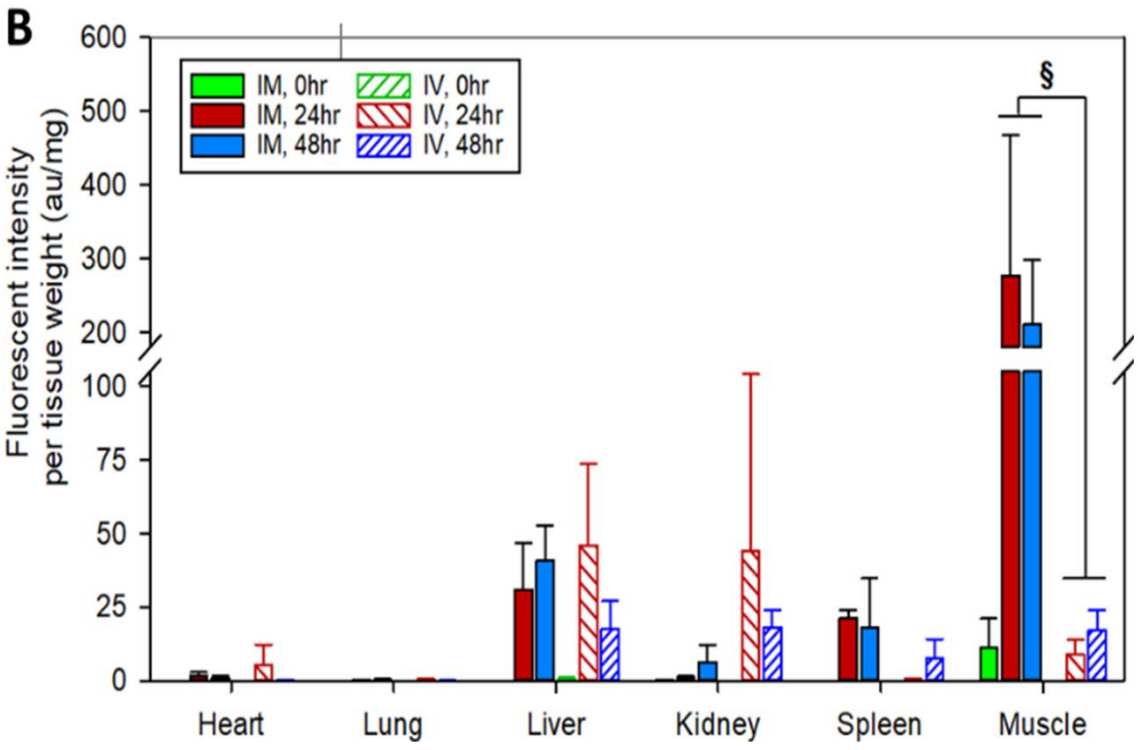
B
IM, 0hr
IM, 24hr
IM, 48hr
IV, 0hr
IV, 24hr
IV, 48hr
§
Fluorescent intensity per tissue weight (au/mg)
600
500
400
300
200
100
75
50
25
0
Heart
Lung
Liver
Kidney
Spleen
Muscle

Figure 10. Biodistribution study of ICG-loaded PLGA nanoparticles through IV and IM injections. A) Fluorescent intensity of collected tissues and organs at different time points; B) Quantification of dye NPs accumulated in tissues and organs at different time points. Data presented as Mean±SD. Student's and Welch's t-test were run and § indicated significant difference ($P<0.01$) with respect to IV injection.

Short-term treatment of SA-10 NPs reduced muscle damage, lung damage, and inflammation in acute limb ischemia model

To test the therapeutic benefits following I/R injury, we administered three IM injections of 64 mg/kg SA-10 NPs at 0 hours, 24 hours, and 48 hours from the start of reperfusion following tourniquet removal. This dosing regimen was chosen based on the drug release profile of the PLGA nanocarrier where ~20% drug release was observed in saline within 12-24 hours. We did not conduct a longer duration study in this model since the limb blood perfusion of tourniquet ligated limbs returns to normal 48 hours after tourniquet removal (Figure 11). We found that SA-10 NPs treatment resulted in a 2-fold reduction in IL-6 protein in hindlimb muscle following injury compared to I/R injury group (Figure 12a). Additionally, only the SA-10 NPs treated group resulted in a 2-fold increase in VEGF protein in hindlimb muscle following injury (Figure 12b). This suggests that treatment with SA-10 NPs reduces inflammatory cytokines and improves endothelial health, evident by the increase in VEGF. Consistent with this, we observed that SA-10 NPs treated gastrocnemius samples had minimal degeneration and necrosis in muscle fibers (Figure 13a, b) as well as dramatically reduced leukocyte infiltration (Figure 13c) compared to the I/R injury group. Lung tissues from the I/R injury group

exhibited damage following skeletal muscle I/R injury, including extensive and focal intra-alveolar edema and hemorrhage, tissue consolidation, and interstitial expansion (Figure 14a). Treatment with SA-10 NPs successfully minimized focal edema, tissue consolidation, and interstitial expansion in lungs following I/R injury (Figure 14b, c), and SA-10 NPs treated lung tissue resembles that of the lung tissue from no injury mice group.

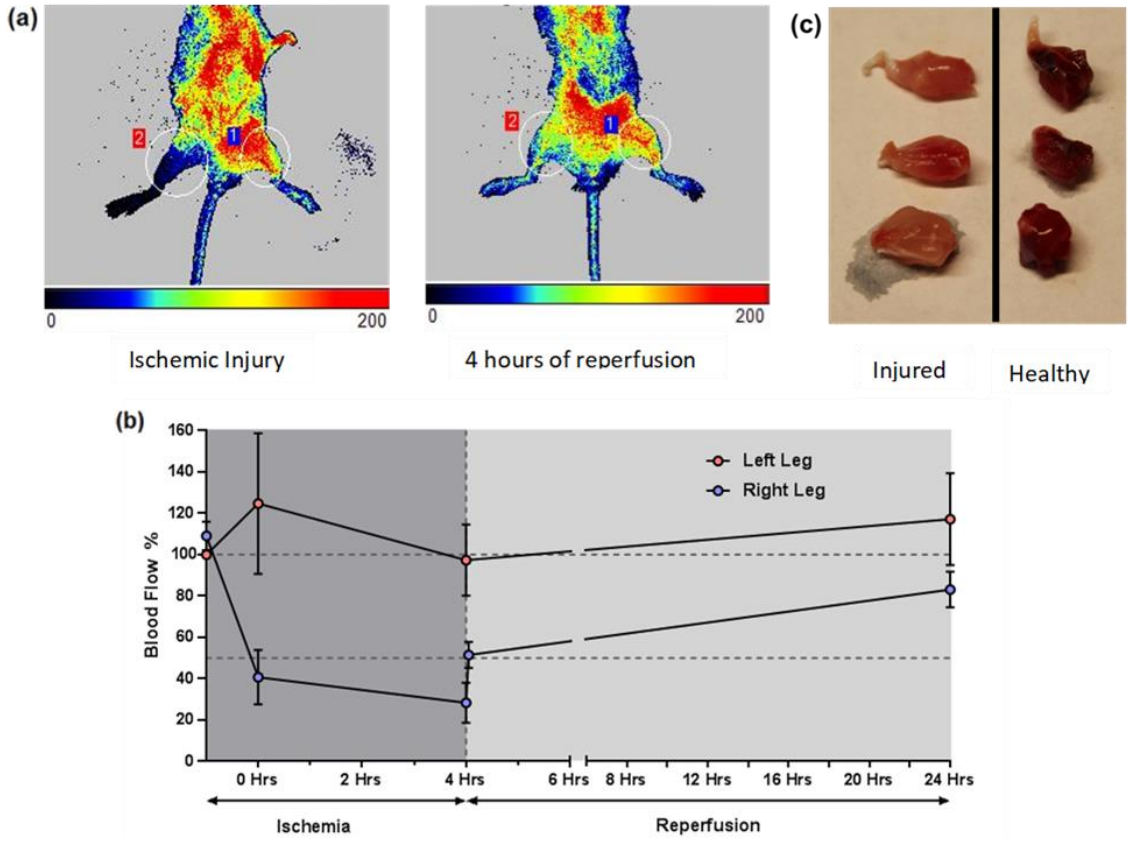

Figure 11. Tourniquet-based acute I/R injury model. (a) Laser Doppler images of hindlimb perfusion during tourniquet-based ischemic injury (left), and 4 hours after tourniquet removal (right). (b) Quantification of laser doppler flowmetry. (c) TTC stain

of gastrocnemius muscles in I/R injured muscles after 24 hours of reperfusion and healthy muscles.

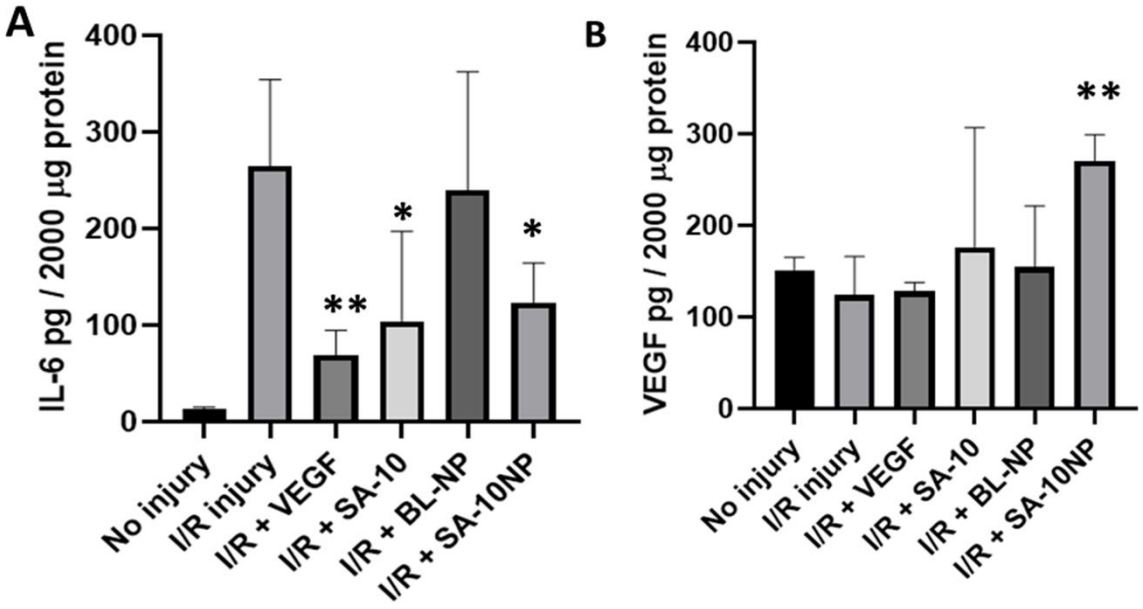

Figure 12. SA-10 NPs decreased inflammation and increased VEGF in a tourniquet induced I/R hindlimb mouse model. A) IL-6 and VEGF (B) measured from the muscle homogenates using ELISA kits. Both SA-10 and SA-10 NPs significantly decreased IL-6 as compared to I/R injured groups. VEGF was significantly increased in SA-10 NPs treated groups. $n \geq 3$, ANOVA followed by Dunnett's test comparisons against I/R injury control were performed. * $p < 0.05$, ** $p < 0.01$, *** $p < 0.001$.

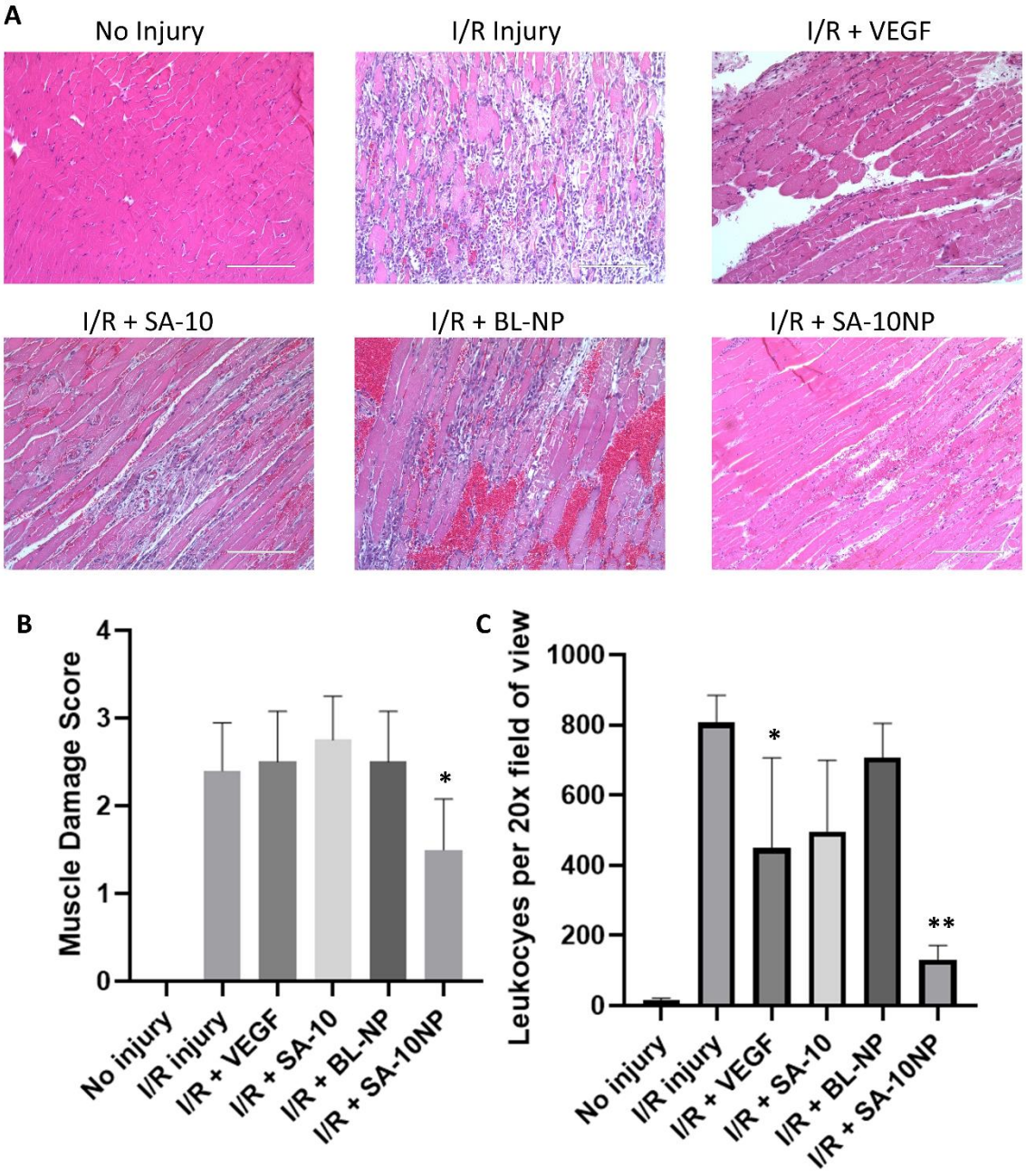

Figure 13. SA-10 NPs decreased muscle damage and leukocyte infiltration in a tourniquet induced I/R hindlimb mouse model. A) Gastrocnemius samples were embedded in paraffin, sectioned, and stained with hematoxylin and eosin, and representative images of tissue sections are shown. B) Qualitative muscle damage was scored. C) Leukocyte

infiltration into muscle per 20x field of view was quantified with ANOVA followed by Dunnett's test comparisons against I/R injury control. $n \geq 3$ * $p < 0.05$, ** $p < 0.001$. Scale bar = 200 µm

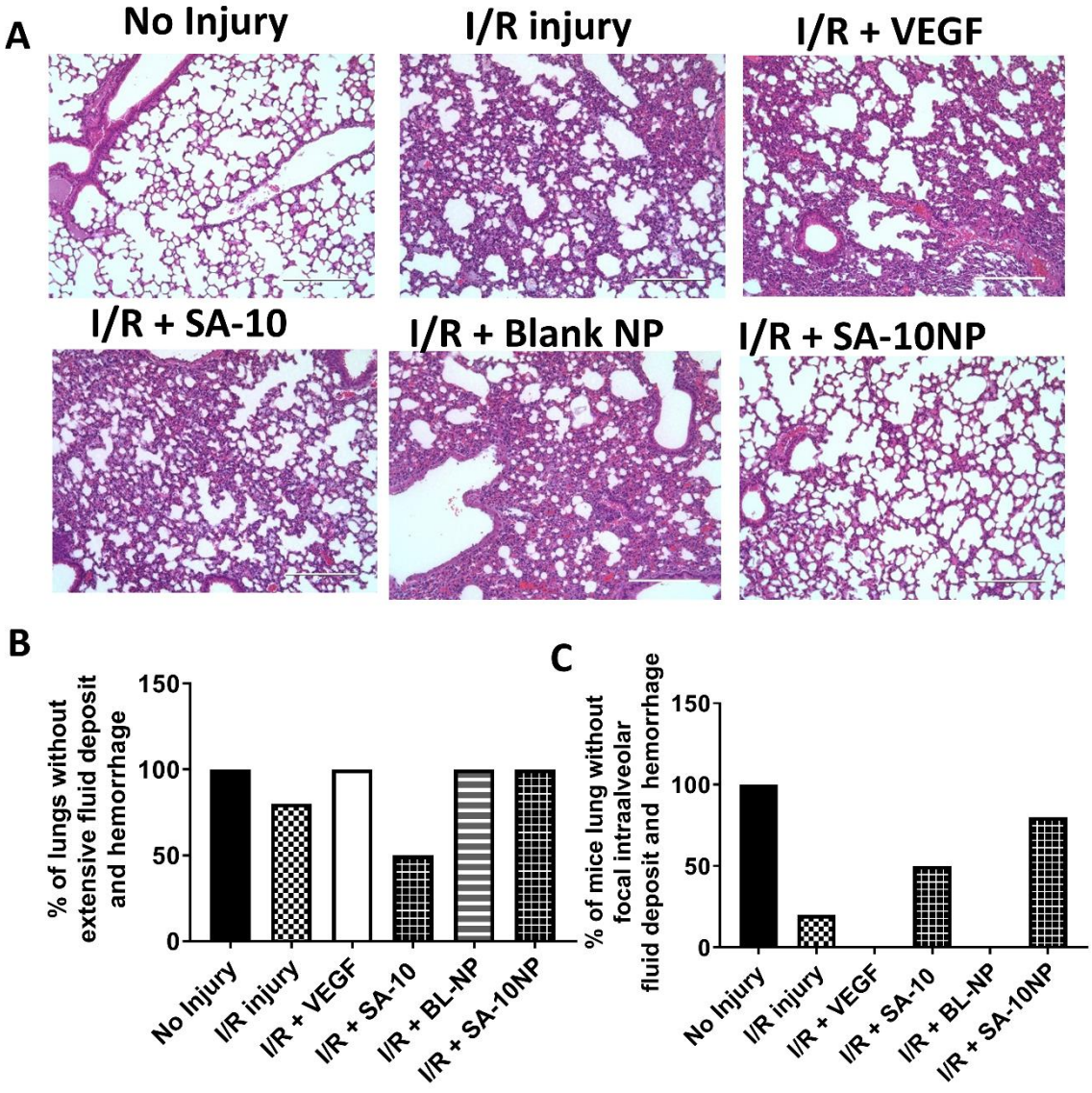

Figure 14. SA-10 NPs decreased lung damage in a tourniquet induced I/R hindlimb mouse model. A) Whole lung tissue samples were embedded in paraffin, sectioned, and stained with hematoxylin and eosin. B) Shows % of mice without extensive interalveolar fluid

deposit and/or hemorrhage. Both VEGF and SA-10 NPs showed 100% protection. C) Shows % of mice without focal lung injury caused by interalveolar fluid deposit and/or hemorrhage. Both SA-10 and SA-10 NPs showed significant protection. n = 3-5, scale bar = 200 μm

Long-term treatment of SA-10 NPs increases blood perfusion and mobility in chronic limb ischemia model

The effective dose of SA-10 NPs was determined to be 16 mg/kg (contained 0.125 mg SA-10/kg) from the dose response study (Figure 15b). At high dose of 128 mg/kg (contained 1.0 mg SA-10/kg) the efficacy was lost possibly due to unknown toxicity indicating 1.0 mg/kg to be the maximum tolerated dose for SA-10 in this model. Therefore, we selected 16 mg/kg dose of SA-10 NPs for the efficacy validation study. The blood perfusion monitored via Laser Speckle Contrast Imaging (LSCI) demonstrated that both SA-10 and SA-10 NPs increased blood perfusion in injured limbs compared to that of injury alone (sham) and blank nanoparticle treatment (Figure 15c). SA-10 NPs also improved blood perfusion significantly in hindlimbs compared to that of free SA-10 and recovered to near normal conditions in 30 days. Sham and blank nanoparticle treated mice were sacrificed after 15-20 days due to the development of necrotic toes, whereas neither SA-10 nor SA-10 NPs treated mice groups developed such signs. Muscle function was assessed by treadmill endurance tests as previously described [137]. We found that both SA-10 and SA-10 NPs treated groups have improved muscle recovery following injury compared to sham and blank nanoparticle treatment groups (Figure 15d) and covered longer distances than the control groups before becoming

exhausted. Additionally, we found that SA-10 NPs treatment was more efficacious in improving muscle recovery compared to that of SA-10.

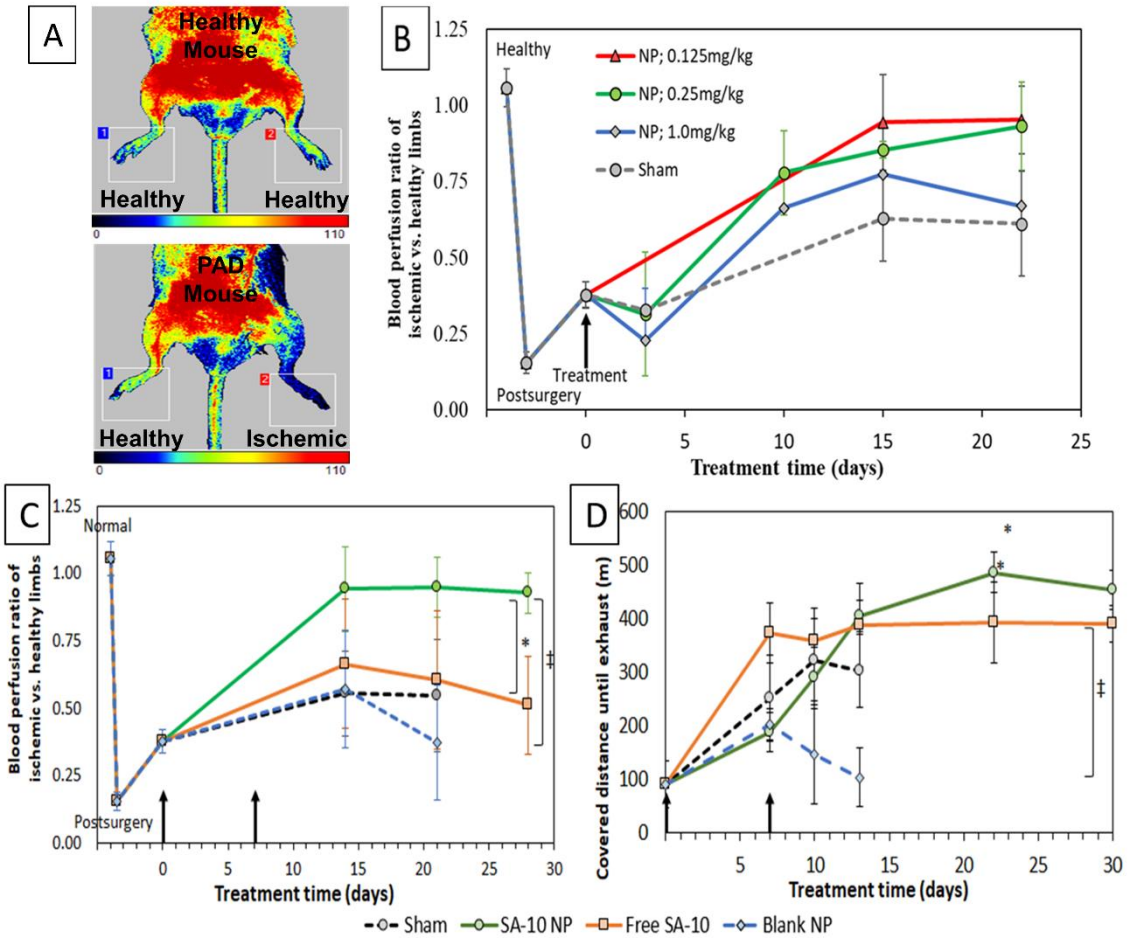

Figure 15. *In vivo* therapeutic effects of SA-10 NPs on mouse hindlimb ischemia models. A) Representative images of mouse hindlimb models: Blue color indicated low blood perfusion while red color indicated high blood perfusion. B) Dose response study of SA-10 NPs: the results determined SA-10 NPs dosed through IM at 16 mg/kg showed highest blood perfusion compared to the other groups. Sham was injected with saline. Blood reperfusion (C) was measured on Laser Speckle Contrast Imaging and quantified as a ratio of blood indexes on ischemic versus normal limbs of the same animal and for

physical recovery (D) The exhaustion test was quantified as ability of the animal to walk (in distance length) on the treadmill until the animals exhausted. * ‡ indicated significant difference ($P<0.05$; n=5) versus sham and blank vehicles, respectively.

Discussion

Our second-generation hybrid NO donor/ROS scavenger molecule, SA-10 containing sulfone functional group exhibited several functional improvements over our previously reported [12] [13] first generation of hybrid molecule, SA-2 containing hydroxylamine functional group (SOD mimetic). Here, we have demonstrated that SA-10 is more potent than SA-2 in protecting EC viability and angiogenesis under in vitro oxidative stress with longer duration of action. Sulfides and sulfones are known to possess the intrinsic capability to scavenge several ROS including hydroxyl radical (HO•), superoxide radical (O2•-), hydrogen peroxide, (H2O2), hypochlorous acid (HOCl), and reactive nitrogen species (RNS), such as nitric oxide (NO•) and peroxynitrite (ONOO•-) produced in excess in the inflammatory site. Fernandes et al. [138] reported that the anti-inflammatory activity of sulindac actually comes from its active metabolites; sulindac sulfides and sulindac sulfones after the parent prodrug sulindac gets metabolized *in vivo* with enhanced radical scavenging activity against both ROS and RNS. Previously, we reported that SA-2 containing an N-OH functional group similar to a well know SOD mimetic, 4-hydroxy tempol scavenged superoxide (O2•) to decreased ROS production following H2O2 treatment in HUVECs [13]. We believe that the superior endothelial cell viability and anti-inflammatory activity demonstrated by the sulfone compound SA-10 is possibly due to scavenging of broad-spectrum ROS and

RNS. The improved protective effects we observe from SA-10 *in vitro* is also consistent with a previous report that the antioxidant capabilities of a molecule correlate with the amount of sulfate groups on that molecule [139].

In the acute I/R injury mice model, an orthodontic elastic band was applied as a tourniquet on the hindlimb close to the pelvic girdle for 4 hours to induce ischemia and then removed to allow for returned blood circulation or reperfusion after 72 hours. This injury model produces several hallmark signs of skeletal muscle IR injury, which includes skeletal muscle injury, sterile inflammation, and remote organ damage. The elevated inflammation induced by skeletal muscle I/R injury can lead to damage in distant organs, of which trauma in lungs is the most common one. Circulating inflammatory cytokines can cause increased lung permeability that leads to edema, interstitial tissue proliferation and expansion, and ultimately lung consolidation. ROS damage cell membranes through lipid peroxidation, and this can be detected by a marked increase in lipid peroxidation products in plasma following I/R injury [94]. Necrotic cell products stimulate the release of inflammatory cytokines such as IL-6, which activate endothelial cells to initiate leukocyte adhesion and promote leukocyte infiltration. Neutrophil activation strongly contributes to endothelial dysfunction and distant organ involvement in that they produce superoxide and hydrogen peroxide and secrete proteases that degrade the tissue basement membrane [95] [96]. Circulating activated neutrophils ultimately leads to lung damage by inducing pulmonary vascular dysfunction and permeability. Treatment with SA-10 NPs minimized each of these complications

following I/R injury, demonstrating SA-10's intrinsic functions as both ROS scavenger and NO donor.

Exogenous NO delivery is a promising therapeutic option in the treatment of I/R injury due to its critical role in vasodilation and vascular health. However, NO donors employed in the treatment of ischemia-related disorders have yielded varying results, ranging from beneficial to toxic. Exogenous supply of nitric oxide has the potential to be harmful depending on the amount of NO delivered as well as the presence of ROS. High doses of NO contribute to inflammation and are ultimately cytotoxic to endothelial cells [86] [87]. Additionally, if NO is delivered in a ROS-rich environment, the two will react to produce peroxynitrite, which is a strong oxidizer that further contributes to lipid peroxidation, mitochondrial dysfunction, and systemic inflammation [127] [128]. ROS surges during I/R injury and overwhelms natural antioxidants such as glutathione. For this reason, it is important to take into consideration ROS levels during I/R injury when delivering low therapeutic doses of NO. Other groups have attempted to address peroxynitrite and other harmful NO metabolite production through highly localized and targeted delivery of NO donors to sites of ischemia, thereby avoiding NO interaction with circulating ROS [140] [99]. Reperfusion following ischemic injury is accompanied by a surge in ROS that damages endothelial cells and initiates harmful inflammatory responses. Injured endothelial cells have then impaired NO production, which limits their ability to survive and revascularize damaged tissue regions. We instead employ the use of a compound SA-10 that is capable of both NO delivery and concomitant ROS scavenging. The increase in VEGF level and decrease in inflammatory cytokine IL-6 in

ischemic muscle tissue after SA-10 treatment might be due a therapeutic level of NO and antioxidants, which minimizes the risk of toxic peroxynitrite metabolites. The *in vivo result* was also supported by the *in vitro* data where we demonstrated SA-10 successfully protects endothelial cells from oxidative stress as well as upregulates the eNOS activity.

We also demonstrated that packaging SA-10 inside PLGA nanoparticles improved the in vivo efficacy of SA-10. We opted to deliver SA-10 NPs intramuscularly in both the acute and chronic limb ischemia models. We found that IV delivery of ICG loaded NPs in a hindlimb ischemia model resulted in moderate accumulation in the liver and kidneys. On the other hand, IM delivery of ICG loaded NPs resulted in a much lower accumulation of NPs in the liver and kidneys as well as a very high concentration in injured hindlimb tissues. Lower accumulation of NPs in uninjured tissues minimizes risk for off-target toxicities. Moreover, hindlimb ischemic injury damages vascular integrity at the injury site, which might prevent proper diffusion of NPs to injured tissues if delivered intravascularly. For these reasons, we selected to deliver SA-10 NPs via IM injections. The decrease in inflammation in muscle tissue as well as leukocyte infiltration in lung tissue combined with decreased lung injury provided the support that this drug delivery technique has broader applicability beyond the targeted ischemic tissue. Delivery of SA-10 NPs might better enable SA-10 to limit circulating ROS and thrombus formation, which could further minimize distant organ damage. Systemic delivery of SA-10 NPs might be more appropriate for other vascular disease models such as coronary artery disease, so further exploration of IV injection of SA-10 NPs and the hemodynamic effects on SA-10 NPs in circulation are needed.

In the chronic hindlimb ischemia model caused after FAL, mice were intramuscularly injected twice at days 0 and 7 with four different treatment group such as saline, blank NPs, SA-10, and SA-10 NPs. Mice treated with saline and blank NPs underwent tissue necrosis, bone exposure, and auto-amputation in the third week, thus no more recovery was recorded. During the 15^{th} 30^{th} days of post injury, mice treated with free SA-10 demonstrated a gradual decrease in the blood perfusion indexes possibly due to rapid clearance of free SA-10 while there was no change in physical endurance test responses. These effects were minimized in animals treated with SA-10 NPs, where SA-10 was gradually released, and significant recovery in both blood perfusion indexes and physical responses were observed.

In summary, our research describes a novel and efficacious therapeutic molecule for the treatment of both acute and chronic ischemia induced limb muscle injury. We demonstrate that the innovative hybrid NO donor/ROS scavenger molecule, SA-10 dosed as a PLGA encapsulated nanosuspension successfully addresses the functional deficits such as poor blood circulation, walking ability, and the underlying molecular pathologies such as increased inflammation, decreased VEGF, and increased tissue damage caused by both NO dysregulation and ROS generation during I/R injury. Ultimately, nanoparticle delivery of SA-10 could greatly benefit patients who suffer from acute limb ischemia as well as distant organ injuries including the lungs. Many elderly patients who suffer from acute limb ischemia cannot undergo surgical or endovascular interventions, so SA-10 NPs fill an important need towards the development of therapeutic alternatives to surgery.

CHAPTER IV

CONCLUSIONS AND FUTURE DIRECTIONS

In project 1, we evaluated SNS control of APC subsets and further explored the SNS as a barrier to anti-tumor immunity by combining the β-blocker propranolol with a therapeutic cancer vaccine. By differentially evaluating $CD115^+$ moMΦ and $CD115^-$ DCs in BMDC cultures, we discovered that true DCs lack β_2ARs and do not experience altered cytokine secretion after norepinephrine treatment. On the other hand, moMΦ do express β_2ARs and are responsive to norepinephrine. Flow cytometry analysis of mouse lymph node and spleen APCs revealed similar findings where macrophages and moDCs exhibit high expression of β_2ARs, whereas β_2ARs were either undetectable or minimally expressed on $CD103^+$, $CD8^+$, plasmacytoid, and $CD11b^+$ DCs. This finding provides important clarification into understanding sympathetic nervous system regulation of APCs. It was previously reported that β_2AR agonist treated BMDCs exhibited altered cytokine secretion and T cell priming, suggesting that DCs are directly regulated at β_2ARs on their surfaces [61]. *In vivo* studies similarly found that increased sympathetic signaling impaired DC maturation and APC priming of T cells, which indirectly supports the claim that DC function can be regulated by β_2ARs at their surfaces [56] [50]. However, we show that norepinephrine regulation of BMDC cultures is due to its impact on $CD115^+$ moMΦ, rather than DCs present in BMDC cultures. Both DCs and moMΦ are critical for priming T cells in paracortex regions of lymph nodes during states of inflammation, but they have been shown to have distinct roles in antigen presentation and T cell priming. Based on our findings, moMΦ appear to be critical mediators of SNS

regulation within the APC compartment. Interestingly, we did find that propranolol-treated mice have enhanced DC maturation following vaccination. This finding suggests that despite their lack of surface β_2ARs, DCs might be indirectly affected by sympathetic regulation, potentially through nearby MCs that are known to influence DC-T cell interactions through local inflammatory responses [52].

We additionally explored the benefit of combining propranolol and a cancer vaccine. We found that this combination treatment dramatically reduced B16-OVA tumor growth compared to vaccination alone. Moreover, this combination resulted in enhanced DC maturation at lymph nodes near the vaccination site and improved systemic IFN-γ responses to the vaccine peptide. The SNS impacts the development of tumor immunity in a multifactorial manner, so we aimed to provide a comprehensive examination of the changes to the tumor immune environment through CyTOF analysis. We found that the combination of propranolol plus vaccine significantly increased intratumor effector $CD8^+$ T cells compared to vaccination alone. We also found that propranolol alone resulted in significantly decreased proportions of PMN and M-MDSCs that express PD-L1, and that the combination group similarly exhibited decreased total PD-$L1^+$ MDSCs among $CD45^+$ cells. This result supports a previously published study that reported β_2ARs expression on MDSCs enhanced their presence in growing tumors, expression of PD-L1, and T cell suppression capabilities [43]. Denervation of sympathetic nerves has been found to reduce M2 TAMs in breast and lung tumor models, resulting in reduced tumor vascularization [29] [11]. While we did not find that addition of propranolol affected the proportion of M2 vs M1 TAM, we did

observe that combination of propranolol plus vaccine resulted in a decrease in TAMs in B16-OVA tumors. Taken together, these results highlight the multifaceted manner in which propranolol can improve anti-tumor immune responses following vaccination.

We expect the field of neuroimmune crosstalk within cancer biology to rapidly develop as cancer immunotherapy strategies advance and become more widely used. To further improve our understanding of SNS regulation of the APC compartment, we expect that methods to visualize spatial organization of cell types within lymph nodes during states of inflammation will greatly elucidate how SNS signaling alters MC recruitment and function within the paracortex region. New techniques including single cell transcriptional mapping and real-time neurochemical detection have been applied to lymph node environments to quantify local cell-to-cell interactions and catecholamine release [141] [17]. We expect these types of high-resolution methods to further improve our understanding of SNS regulation of the lymph node environment. Combination of β-blockers and cancer immunotherapies will likely receive more exploration, especially with the ongoing phase Ib/II clinical trial testing the combination of propranolol and the αPD-1 monoclonal antibody, pembrolizumab (NCT03384836). An important step in advancing the use of β-blockers and cancer immunotherapies towards clinical application is to evaluate the minimum dose of a β-blocker needed to impact immune cell function in humans. Murine models utilizing propranolol to impact immune cells typically use 10 mg/kg doses daily, which is a much higher weight dose than that given to humans, which commonly range from 40-240 mg total every 12 hours. Retrospective studies examining incidental use of β-blockers prior to cancer immunotherapy do

suggest that these doses will beneficially impact the development of tumor immunity [142], but more rigorous evaluation of minimal effective doses for propranolol are needed.

In project 2, we evaluated our novel hybrid drug SA-10 that can deliver therapeutic doses of NO while also minimizing local oxidative stress for the treatment of limb I/R injury. This drug design exhibits significant improvements over its predecessor SA-2 through enhanced protection of endothelial cell health under oxidative stress *in vivo*. To improve drug stability and sustained delivery, we packaged SA-10 in PLGA nanoparticles. We treated two different models of murine hindlimb ischemia and found that SA-10NPs minimized local and distant tissue damage, improved muscle function and perfusion, and reduced local inflammation following injury. These results show that nanoparticle delivery of SA-10 could greatly benefit patients who suffer from acute limb ischemia and might minimize the risk of distant organ damage following reperfusion injury.

To further improve the efficacy of SA-10NPs, we plan to evaluate the hemodynamic effects on SA-10NPs to prepare for IV application of the drug. Since our models of limb ischemia resulted in severely impaired blood perfusion into the injured tissues, we elected to directly inject SA-10NPs into mouse gastrocnemius muscles. However, IV application of SA-10NPs will be necessary for the treatment of reperfusion injury in cerebral, cardiac, or diffuse gastric ischemia. For these reasons, we plan to address safety profiles, minimum effective dose, and pharmacodynamic properties of SA-10NPs when injected IV in future studies.

In summary, we provide evidence to support the combination of propranolol and a cancer vaccine for the treatment of melanoma in project 1. Our discovery that β_2AR signaling impacts moMΦ, but not DCs in BMDC cultures also highlights the need to address BMDC heterogeneity when studying DC biology. We additionally demonstrate that the novel hybrid drug SA-10 is a promising treatment option for chronic and acute cases of limb ischemia injury in project 2. SA-10NP provides a nonsurgical option for limb ischemia treatment, and it addresses the molecular mechanisms that underly reperfusion injury.

REFERENCES

[1] S. Cole, A. Nagaraja, S. Lutgendorf, P. Green and A. Sood, "Sympathetic nervous system regulation of the tumour microenvironment," *Nature Reviews Cancer,* vol. 15, no. 9, pp. 563-572, 2015.

[2] C. Magnon, S. Hall, J. Lin, X. Xue, L. Gerber, S. Freedland and P. Frenette, "Autonomic Nerve Development Contributes to Prostate Cancer Progression," *Science,* vol. 341, no. 6142, 2013.

[3] J. Pundavela, S. Roselli, S. Faulkner, J. Attia, R. Scott, R. Thorne, J. Forbes, R. Bradshaw, M. Walker, P. Jobling and H. Hondermarck, "Nerve fibers infiltrate the tumor microenvironment and are associated with nerve growth factor production and lymph node invasion in breast cancer," *Molecular Oncology,* vol. 9, pp. 1626-1635, 2015.

[4] F. Liebl, I. E. Demir, R. Rosenberg, A. Boldis, E. Yildiz, K. Kujundzic, T. Kehl, D. Dischl, T. Schuster, M. Maak, K. Becker, R. Langer, M. Laschinger, H. Friess and G. Ceyhan, "The Severity of Neural Invasion Is Associated with Shortened Survival in Colon Cancer," *Clinical Cancer Research,* vol. 19, no. 1, pp. 50-61, 2012.

[5] V. De Giorgi, M. Grazzini, S. Benemei, N. Marchionni, E. Botteri, E. Pennacchioli, P. Geppetti and S. Gandini, "Propranolol for Off-label Treatment of

Patients With Melanoma," *JAMA Oncology,* vol. 4, no. 2, pp. e172908-e172908, 2018.

[6] H. M. Wang, Z. X. Liao, R. Komaki, J. W. Welsh, M. S. O'Reilly, J. Y. Chang, Y. Zhuang, L. B. Levy, C. Lu and D. R. Gomez, "Improved survival outcomes with the incidental use of beta-blockers among patients with non-small-cell lung cancer treated with definitive radiation therapy," *Annals of Oncology,* vol. 24, no. 5, pp. 1312-1319, 2013.

[7] L. Jansen, M. Hoffmeister, V. Arndt, J. Chang-Claude and H. Brenner, "Stage-Specific Associations Between Beta Blocker Use and Prognosis After Colorectal Cancer," *Cancer,* vol. 120, no. 8, pp. 1178-1186, 2014.

[8] M. Chen, G. Qiao, B. Hylander, H. Mohammadpour, X.-Y. Wang, J. Subjeck, A. Singh and E. Repasky, "Adrenergic stress constrains the development of anti-tumor immunity and abscopal responses following local radiation," *Nature Communications,* vol. 11, no. 1, pp. 1-12, 2020.

[9] M. Bucsek, G. Qiao, C. MacDonald, ... and E. Repasky, "[Beta]-adrenergic signaling in mice housed at standard temperatures suppresses an effector phenotype in CD8+ T cells and undermines checkpoint inhibitor therapy," *Cancer Research,* vol. 77, no. 20, pp. 5639-5651, 2017.

[10] H. Mohammadpour, C. MacDonald, G. Qiao, M. Chen, B. Dong, B. Hylander, P. McCarthy, S. Abrams and E. Repasky, "[Beta]2 adrenergic receptor-mediated signaling regulates the immunosuppressive potential of myeloid-derived

suppressor cells," *Journal of Clinical Investigation,* vol. 129, no. 12, pp. 5537-5552, 2019.

[11] Y. Xia, Y. Wei, Z.-Y. Li, X.-Y. Cai, L.-L. Zhang, X.-R. Dong, S. Zhang, R.-G. Zhang, R. Meng, F. Zhu and G. Wu, "Catecholamines contribute to the neovascularization of lung cancer via tumor-associated macrophages," *Brain, Behavior, and Immunity,* vol. 81, pp. 111-121, 2019.

[12] S. Acharya, P. Rogers, R. Krishnamoorthy, ... and T. Yorio, "Design and synthesis of novel hybrid sydnonimine and prodrug useful for glaucomatous optic neuropathy," *Bioorganic & Medicinal Chemistry Letters*, vol. 26, no. 5, pp. 1490-1494, 2016.

[13] D. Le, A. Kurisakose, D. Nguyen, K. Nguyen and S. Acharya, "Hybrid Nitric Oxide Donor and its Carrier for the Treatment of Peripheral Arterial Diseases," *Scientific Reports,* vol. 7, no. 8692, 2017.

[14] V. Pavlov, S. Chavan and K. Tracy, "Molecular and Functional Neuroscience in Immunity," *Annual Review of Immunology,* vol. 36, pp. 783-812, 2018.

[15] C. Scheiermann, Y. Kunisaki, D. Lucas, A. Chow, J.-E. Jang, D. Zhang, D. Hashimoto, M. Merad and P. Frenette, "Adrenergic Nerves Govern Circadian Leukocyte Recruitment to Tissues," *Immunity,* vol. 37, no. 2, pp. 290-301, 2012.

[16] E. Sloan, J. Capitanio, R. Tarara and S. Cole, "Social temperament and lymph node innervation," *Brain, Behavior, and Immunity,* vol. 22, no. 5, pp. 717-726, 2008.

[17] G. Lim, S. Regan and A. Ross, "Subsecond spontaneous catecholamine release in mesenteric lymph nod ex vivo," *Journal of Neurochemistry,* vol. 115, pp. 417-429, 2020.

[18] J. Benovic, "Novel [Beta2]-adrenergic receptor signaling pathways," *Journal of Allergy and Clinical Immunology,* vol. 110, no. 6, pp. S229-S235, 2002.

[19] M. Szpunar, E. Belcher, R. Dawes and K. Madden, "Sympathetic innervation, norepinephrine content, and norepinephrine turnover in orthotopic and spontaneous models of breast cancer," *Brain, Behavior, and Immunity,* vol. 53, pp. 223-233, 2016.

[20] M. Amit, H. Takahashi, M. Dragomir, ... and J. Myers, "Loss of p53 drives neuron reprogramming in head and neck cancer," *Nature,* vol. 578, pp. 449-454, 2020.

[21] C. Liebig, G. Ayala, J. Wilks, D. Berger and D. Albo, "Perineural Invasion in Cancer," *Cancer,* pp. 3379-3391, 2009.

[22] A. Zahalka and P. Frenette, "Nerves in Cancer," *Nature Reviews Cancer,* vol. 20, pp. 143-157, 2020.

[23] G. Ayala, H. Dai, M. Powell, R. Li, Y. Ding, T. Wheeler, D. Shine, D. Kadmon, T. Thompson, B. Miles, M. Ittmann and D. Rowley, "Cancer-Related Axonogenesis and Neurogenesis in Prostate Cancer," *Human Cancer Biology,* vol. 14, no. 23, pp. 7593-7603, 2008.

[24] A. Kamiya, Y. Hayama, S. Kato, A. Shimomura, T. Shimomura, K. Irie, R. Kaneko, Y. Yanagawa, K. Kobayashi and T. Ochiya, "Genetic manipulation of autonomic nerve fiber innervation and activity and its effect on breast cancer progression," *Nature Neuroscience,* vol. 22, no. 8, pp. 1289-1305, 2019.

[25] B. Renz, T. Tanaka, M. Sunagawa, ... and T. Wang, "Cholinergic Signaling via Muscarinic Receptors Directly and Indirectly Suppresses Pancreatic Tumorigenesis and Cancer Stemness," *Cancer Discovery,* vol. 8, pp. 1458-1473, 2018.

[26] L. I. Partecke, A. Käding, D. N. Trung, ... and W. Keßler, "Subdiaphragmatic vagotomy promotes tumor growth and reduces survival via TNFα in a murine pancreatic cancer model," *Oncotarget,* vol. 8, no. 14, pp. 22501-22512, 2017.

[27] C.-M. Zhao, Y. Kodama, S. Muthupalani, C. Westphalen, G. Andersen, A. Flatberg, H. Johannessen, ..., T. Wang and D. Chen, "Denervation suppresses gastric tumorigenesis," *Sci Transl Med,* vol. 6, no. 250, 2014.

[28] P. Thaker, L. Han, A. Kamat, ... and A. Sood, "Chronic stress promotes tumor growth and angiogenesis in a mouse model of ovarian carcinoma," *Nature Medicine,* vol. 12, no. 8, pp. 939-944, 2006.

[29] E. Sloan, S. Priceman, B. Cox, ... and S. Cole, "The Sympathetic Nervous System Induces a Metastatic Switch in Primary Breast Cancer," *Cancer Research,* vol. 70, pp. 7042-7052, 2010.

[30] J. Folkman, K. Watson, D. Ingber and D. Hanahan, "Induction of angiogenesis during the transition from hyperplasia to neoplasia," *Nature,* vol. 339, pp. 58-61, 1989.

[31] A. Zahalka, A. Arnal-Estape, M. Maryanovich, F. Nakahara, C. Cruz, L. Finley and P. Frenette, "Adrenergic nerves activate an angio-metabolic switch in prostate cancer," *Science,* vol. 358, pp. 321-326, 2017.

[32] C. Le, C. Nowell, C. Kim-Fuchs, ... and E. Sloan, "Chronic stress in mice remodels lymph vasculature to promote tumor cell dissemination," *Nature Communications,* vol. 7, no. 10634, 2016.

[33] G. Armaiz-Pena, J. Allen, A. Cruze, ... and A. Sood, "Src activation by [beta]-adrenoreceptors is a key switch for tumor metastasis," *Nature Communications,* vol. 4, no. 1403, 2012.

[34] M. Nilsson, G. Armaiz-Pena, R. Takahashi, ... and A. Sood, "Stress Hormones Regulate Interleukin-6 Expression by Human Ovarian Carcinoma Cells through a Src-dependent Mechanism," *The Journal of Biological Chemistry,* vol. 282, no. 41, pp. 29919-29926, 2007.

[35] M. Shahzad, J. Arevalo, G. Armaiz-Pena, ... and A. Sood, "Stress Effects on FosB- and Interleukin-8 (IL-8)-driven Ovarian Cancer Growth and Metastasis," *The Journal of Biological Chemistry,* vol. 285, no. 46, pp. 35462-35470, 2010.

[36] M. Shi, H. Duan, L. Qian, ... and N. Guo, "The [beta]2-adrenergic receptor and Her2 comprise a positive feedback loop in human breast cancer cells," *Breast Cancer Research and Treatment,* vol. 125, pp. 351-362, 2011.

[37] L. Gu, S. Lau, S. Loera, G. Somlo and S. Kane, "Protein Kinase A Activation Confers Resistance to Trastuzumab in Human Breast Cancer Cell Lines," *Clinical Cancer Research,* vol. 15, no. 23, pp. 7196-7206, 2009.

[38] M. Hara, J. Kovacs, E. Whalen, ... and R. Lefkowitz, "A stress response pathway regulates DNA damage through [beta]2-adrenoreceptors and [beta]-arrestin-1," *Nature,* vol. 477, pp. 349-353, 2011.

[39] A. Reeder, M. Attar, L. Nazario, ... and M. S. Flint, "Stress hormones reduce the efficacy of paclitaxel in triple negative breast cancer through induction of DNA damage," *British Journal of Cancer,* vol. 112, pp. 1461-1470, 2015.

[40] R. Glaser and J. Kiecolt-Glaser, "Stress-induced immune dysfunction: implications for health," *Nature Reviews Immunology,* vol. 5, pp. 243-251, 2005.

[41] D. Felten and S. Felten, "Sympathetic noradrenergic innervation of immune organs," *Brain, Behavior, and Immunity,* vol. 2, no. 4, pp. 293-300, 1988.

[42] F. Veglia, M. Perego and Gabrilovich, "Myeloid-derived suppressor cells coming of age," *Nature Immunology,* vol. 19, pp. 108-119, 2018.

[43] H. Mohammadpour, C. MacDonald, G. Qiao, M. Chen, B. Dong, B. Hylander, P. McCarthy, S. Abrams and E. Repasky, "[Beta]2 adrenergic receptor-mediated

signaling regulates the immunosuppressive potential of myeloid-derived suppressor cells," *Journal of Clinical Investigation,* Vols. In-Press Review, 2019.

[44] R. Noy and J. Pollard, "Tumor-Associated Macrophages: From Mechanisms to Therapy," *Immunity,* vol. 41, pp. 49-61, 2014.

[45] D. Lamkin, H.-Y. Ho, T. Ong, C. Kawanishi, V. Stoffers, N. Ahlawat, J. Ma, J. Arevalo, S. Cole and E. Sloan, "Beta adrenergic-stimulated macrophages: Comprehensive localization in the M1-M2 spectrum," *Brain, Behavior, and Immunity,* vol. 57, pp. 338-346, 2016.

[46] A. Smith, J. Qualls, K. O'Brien, L. Balouzian, P. Johnson, S. Schultz-Cherry, S. Smale and P. Murray, "A Distal Enhancer in IL12b Is the Target of Transcriptional Repression by the STAT3 Pathway and Requires the Basic Leucine Zipper (B-ZIP) Protein NFIL3," *The Journal of Biological Chemistry ,* vol. 286, no. 26, pp. 23582-23590, 2011.

[47] V. Sanders, "The Beta2-Adrenergic Receptor on T and B Lymphocytes: Do We Understand It Yet?," *Brain, Behavior, and Immunity,* vol. 26, no. 2, pp. 195-200, 2012.

[48] D. S. Ramer-Quinn, R. Baker and V. Sanders, "Activated T Helper 1 and T Helper 2 Cells Differentially Express the [beta]-2-Adrenergic Receptor: A Mechanism for Selective Modulation of T Helper 1 Cell Cytokine Production," *Journal of Immunology ,* vol. 159, pp. 4857-4867, 1997.

[49] C. Daher, L. Vimeux, R. Stoeva, E. Peranzoni, G. Bismuth, E. Wieduwild, B. Lucas, E. Donnadieu, N. Bercovici, A. Trautmann and V. Feuillet, "Blockade of [Beta]-Adrenergic Receptors Improves CD8+ T-cell Priming and Cancer Vaccine Efficacy," *Cancer Immunology Research,* vol. 7, no. 11, 2019.

[50] K. Grebe, H. Hickman, K. Irvine, K. Takeda, J. Bennink and J. Yewdell, "Sympathetic nervous system control of anti-influenza CD8+ T cell responses," *PNAS,* vol. 106, no. 13, pp. 5300-5305, 2009.

[51] E. Sternberg, "Neural regulation of innate immunity: a coordinated nonspecific host response to pathogens," *Nature Reviews Immunology,* vol. 6, no. 4, pp. 318-328, 2006.

[52] J. Leal, J. Huang, K. Kohli, C. Stoltzfus, M. Lyons-Cohen, B. Olin, M. Gale and M. Gerner, "Innate cell microenvironemnts in lymph nodes shape the generation of T cell responses during type I inflammation," *Science Immunology,* vol. 6, no. 56, 2021.

[53] K.-L. Chu, B. Nathália, M. Girard and T. Watts, "Monocyte-Derived Cells in Tissue-Resident Memory T Cell Formation," *Journal of Immunology,* vol. 204, no. 3, pp. 447-485, 2020.

[54] G. Bellingan, H. Caldwell, S. Howie, I. Dransfield and C. Haslett, "In vivo fate of the inflammatory macrophage during the resolution of inflammation: inflammatory macrophages do not die locally, but emigrate to the draining lymph nodes.," *Journal of Immunology,* vol. 157, no. 6, pp. 2577-2585, 1996.

[55] K. Hilligan, S.-C. Tang, E. Hyde, ... and F. Ronchese, "Dermal IRF4+ dendritic cells and monocytes license CD4+ T helper cells to distinct cytokine profiles," *Nature Communications,* vol. 11, no. 5637, pp. 1-14, 2020.

[56] K. Kokolus, H. Spangler, B. Povinelli, ... and E. Repasky, "Stressful presentations: mild cold stress in laboratory mice influences phenotype of dendritic cells in naive and tumor-bearing mice," *Frontiers in Immunology,* vol. 5, 2014.

[57] M. Lutz, N. Kukutsch, A. Ogilvie, S. Roßner, F. Koch, N. Romani and G. Schuler, "An advanced culture method for generating large quantities of highly pure dendritic cels form mouse bone marrow," *Journal of Immunological Methods,* vol. 223, no. 1, pp. 77-92, 1999.

[58] K. Inaba, M. Inaba, N. Romani, H. Aya, M. Deguchi, S. Ikehara, S. Muramatsu and R. Steinman, "Generation of large numbers of Dendritic Cells from Mouse Bone Marrow Cultures Supplemented with Granulocyte/Macrophage Colony-stimulating Factor," *Journal of Experimental Medicine,* vol. 176, no. 6, pp. 1693-1702, 1992.

[59] J. Helft, J. Bottcher, P. Chakravarty, S. Zelenay, J. Huotari, B. G. D. Schraml and C. Reis e Sousa, "GM-CSF Mouse Bone Marrow Cultures Comprise a Heterogeneous Population of CD11c+MHCII+ Macrophages and Dendritic Cells," *Immunity,* vol. 42, no. 6, pp. 1197-1211, 2015.

[60] Y. R. Na, D. Jung, G. J. Gu and S. H. Seok, "GM-CSF Grown Bone Marrow Derived Cells Are Composed of Phenotypically Different Dendritic Cells and Macrophages," *Mol. Cells,* vol. 39, no. 10, pp. 734-741, 2016.

[61] M. Takenaka, L. Araujo, J. Maricato, V. Nasciemento, M. Guereschi, R. Rezende, F. Quintana and A. Basso, "Norepinephrine Controls Effector T Cell Differentiation through [Beta]2-Adrenergic Receptor-Mediated Inibition of NF-[kappa]B and AP-1 in Dendritic Cells," *The Journal of Immunology,* vol. 196, pp. 637-644, 2016.

[62] G. Maestroni, "Short exposure of maturing, bone marrow-derived dendritic cells to norepinephrine: impact on inetic of cytokine production and Th development," *Journal of Neuroimmunology,* vol. 129, no. 1-2, pp. 106-114, 2002.

[63] Y. Yanagawa, M. Matsumoto and H. Togashi, "Adrenoreceptor-mediated enhancement of interleukin-33 production by dendritic cells," *Brain, Behavior, and Immunity,* vol. 25, pp. 1427-1433, 2011.

[64] H. Wu, J. Chen, S. Song, ... and W. Wei, "β 2-adrenoceptor signaling reduction in dendritic cells is involved in the inflammatory response in adjuvant-induced arthritic rats," *Scientific reports,* vol. 6, no. 1, pp. 1-11, 2016.

[65] E. Yang, S.-j. K. Kim, E. Donovan, M. Chen, A. Gross, J. Webster Marketon, S. Barsky and R. Glaser, "Norepinephrine upregulates VEGF, IL-8, and IL-6 expression in human melanoma tumor cell lines: implications for stress-related

enhancement of tumor progression," *Brain, Behavior, and Immunity,* vol. 23, no. 2, pp. 267-275, 2009.

[66] T. Ben-Shaanan, M. Schiller, H. Azulay-Debby, B. Korin, N. Boshnak, T. Koren, M. Krot, J. Shakya, M. Rahat, F. Hakim and A. Rolls, "Modulation of anti-tumor immunity by the brain's reward system," *Nature Communications,* vol. 9, no. 2723, pp. 1-10, 2018.

[67] R. Ammi, J. De Waele, Y. Willemen, I. Van Brussel, D. Schrijvers, E. Lion and E. Smits, "Poly(I:C) as cancer vaccine adjuvant: Knocking on the door of medical breakthroughs," *Pharmacology & Therapeutics,* vol. 146, pp. 120-131, 2015.

[68] H. B. Levy, G. Baer, S. Baron, C. E. Buckler, C. J. Gibbs, M. J. Iadarola, W. T. London and J. Rice, "A Modified Polyriboinosinic-Polyribocytidylic Acid Complex That Induces Interferon in Primates," *The Journal of Infectious Diseases,* vol. 132, no. 4, pp. 434-439, 1975.

[69] M. Girard-Madoux, J. Kel, B. Reizis and B. Clausen, "IL-10 controls dendritic cell-induced T-cell reactivition in the skin to limit contact hypersensitivity," *The Journal of Allergy and Clinical Immunology*, vol. 129, no. 1, pp. 143-150, 2012.

[70] T. Koya, H. Matsuda, T. Katsuyuki, S. Matsubara, N. Miyahara, A. Balhorn, A. Dakhama and E. Gelfand, "IL-10-treated dendritic cells decrease airway hyperresponsiveness and airway inflammation in mice," *The Journal of Allergy and Clinical Immunology* , vol. 119, no. 5, pp. 1241-1250, 2007.

[71] I. Monteleone, A. Platt, E. Jaensson, W. Agace and A. Mowat, "IL-10-dependent partial refractoriness to Toll-like receptor stimulation modulates gut mucosal dendritic cell function," *European Journal of Immunology,* vol. 38, pp. 1533-1547, 2008.

[72] K. Steinbrink, M. Wolfl, H. Jonuleit, J. Knop and A. Enk, "Induction of Tolerance by IL-10-Treated Dendritic Cells," *The Journal of Immunology,* vol. 159, pp. 4772-4780, 1997.

[73] C. Woiciechowsky, K. Asadullah, D. Nestler, B. Eberhardt, C. Platzer, B. Schoning, F. Glockner, W. Lanksch, H.-D. Volk and W.-D. Docke, "Sympathetic activation triggers systemic interleukin-10 release in immunodpression induced by brain injury," *Nature Medicine,* vol. 4, no. 7, pp. 808-813, 1998.

[74] C. Porta, F. Consonni, S. Morlacchi, ... and A. Sica, "Tumor-Derived Prostaglandin E2 Promotes p50 NF-kB-Dependent Differentiation of Monocytic MDSCs," *Cancer Research* , vol. 80, no. 13, pp. 2874-2888, 2020.

[75] J. Herve, L. Dubreil, V. Tardif, ... and P. Blancou, "Beta2-adrenoreceptor agonist inhibits antigen cross-presentation by dendritic cells," *The Journal of Immunology,* vol. 190, pp. 3163-3171, 2013.

[76] A. Sommershof, L. Scheuermann, ... and M. Groettrup, "Chronic stress suppresses anti-tumor TCD8+ responses and tumor regression following cancer immunotherapy in a mouse model of melanoma," *Brain, Behavior, and Immunity,* vol. 65, pp. 140-149, 2017.

[77] Y.-L. Su, S. Banerjee, S. V. White and M. Kortylewski, "STAT3 in Tumor-Associated Myeloid Cells: Multitasking to Disrupt Immunity," *International Journal of Molecular Sciences,* vol. 19, no. 6, p. 1803, 2018.

[78] A. Dua and C. Lee, "Epidemiology of Peripheral Arterial Disease and Critical Limb Ischemia," *Techniques in Vascular and Interventional Radiology,* vol. 19, no. 2, pp. 91-95, 2016.

[79] F. G. R. Fowkes, D. Rudan, I. Rudan, ... and M. Criqui, "Comparison of global estimates of prevalence and risk factors for peripheral artery disease in 2000 and 2010: a systematic review and analysis," *The Lancet,* vol. 382, no. 9901, pp. 1329-1340, 2013.

[80] J. Shu and G. Santulli, "Update on peripheral artery disease: Epidemiology and evidence-based facts," *Atherosclerosis,* vol. 275, pp. 379-381, 2018.

[81] A. Go, D. Mozaffarian, V. Roger, ... and M. Turner, "Heart Disease and Stroke Statistics," *Circulation,* vol. 129, pp. e28-e292, 2014.

[82] K. Ouriel, "Peripheral arterial disease," *The Lancet,* vol. 358, no. 9289, pp. 1257-1264, 2001.

[83] E. B. Jude, I. Eleftheriadou and N. Tentolouris, "Peripheral arterial disease in diabetes-a review," *Diabetic Medicine,* vol. 27, pp. 4-14, 2010.

[84] C. Collard and S. Gelman, "Pathophysiology, Clinical Manifestations, and Prevention of Ischemia-Reperfusion Injury," *Anesthesiology,* vol. 94, pp. 1133-1138, 2001.

[85] D. Carden and D. Granger, "Pathophysiology of ischaemia-reperfusion injury," *Journal of Pathology,* vol. 190, pp. 255-266, 2000.

[86] G. Fantini and M. Conte, "Pulmonary failure following lower torso ischemia: clinical evidence for a remote effect of reperfusion injury.," *The American Surgeon,* vol. 61, no. 4, pp. 316-319, 1995.

[87] D. Tousoulis, A. Kampoli, C. Tentolouris, N. Papageorgiou and C. Stefanadis, "The role of nitric oxide on endothelial function," *Current Vascular Pharmacology,* vol. 10, no. 1, pp. 4-18, 2012.

[88] A. Khanna, P. Cowled and R. Fitridge, "Nitric Oxide and Skeletal Muscle Reperfusion Injury: Current Controversies (Research Review)," *Journal of Surgical Research,* vol. 128, pp. 98-107, 2005.

[89] M. Ozaki, S. Kawashima, T. Hirase and e. al., "Overexpression of endothelial nitric oxide synthase in endothelial cells is protective against ischemia-reperfusion injury in mouse skeletal muscle," *American Journal of Pathology,* vol. 160, p. 1335, 2002.

[90] J. Barker, K. Knight, R. Romeo and e. al., "Targeted disruption of the nitric oxide synthase 2 gene protects against ischaemia/reperfusion injury to skeletal muscle," *Journal of Pathology,* vol. 194, p. 109, 2001.

[91] L. Terada, J. Dormish, P. Shanley, J. Leff, B. Anderson and J. Repine, "Circulation xanthine oxidase mediates lung neutrophil sequestration after

intestinal ischemia-reperfusion," *Journal of Physiology,* vol. 263, pp. L394-L401, 1992.

[92] E. Chouchani, V. Pell, A. James, ... and M. Murphy, "A Unifying Mechanism for Mitochondrial Superoxide Production during Ischemia-Reperfusion Injury," *Cell Metabolism,* vol. 23, no. 2, pp. 254-263, 2016.

[93] M. Murphy, "How mitochondria produce reactive oxygen species," *Biochemical Journal,* vol. 417, no. 1, pp. 1-13, 2009.

[94] S. Toyokuni, "Reactive oxygen species-induced molecular damage and its application in pathology," *Pathology International* , vol. 49, pp. 91-102, 1999.

[95] D. Carden, F. Xiao, C. Moak, B. Willis, S. Robinson-Jackson and S. Alexander, "Neutrophil elastase promotes lung microvascular injury and proteolysis of endothelial cadherins," *American Journal of Physiology,* vol. 275, pp. H385-H392, 1998.

[96] F. Xiao, M. Eppihimer, J. Young, K. Nguyen and D. Carden, "Lung neutrophil retention and injury following intestinal ischemia-reperfusion," *Microcirculation,* vol. 4, pp. 359-367, 1997.

[97] T. Bisdas, M. Borowski and G. Torsello, "Current practice of first-line treatment strategies in patients with critical limb ischemia," *Journal of Vascular Surgery,* vol. 62, no. 4, pp. 965-972, 2015.

[98] G. Chen, M. Thakkar, C. Robinson and S. Dore, "Limb Remote Ischemic Conditioning: Mechanisms, Anesthetics, and the Potential for Expanding Therapeutic Options," *Frontiers in Neurology,* vol. 9, no. 40, 2018.

[99] M. Navati, A. Lucas, C. Liong, ... and P. Cabrales, "Reducing Ischemia/Reperfusion Injury by the Targeted Deliver of Nitric Oxide from Magnetic-Field-Induced Localization of S-Nitrosothiol-Coated Paramagnetic Nanoparticles," *ACS Applied Bio Materials*, vol. 2, no. 7, pp. 2907-2919, 2019.

[100] T. Senoner, S. Schindler, S. Stättner, D. Öfner, J. Troppmair and F. Primavesi, "Associations of Oxidative Stress and Postoperative Outcome in Liver Surgery with an Outlook to Future Potential Therapeutic Options," *Oxidative Medicine and Cellular Longevity,* vol. 2019, 2019.

[101] T. Asahara, C. Bauters, Pastore, ... and J. Isner, "Local Delivery of Vascular Endothelial Growth Factor Accelerates Teendothelialization and Attentuates Intimal Hyperplasia in Ballon-Injured Rat Carotid Artery," *Circulation,* vol. 91, pp. 2793-2801, 1995.

[102] M. Laitinen, I. Zachary, G. Breier, T. Pakkanen, ... and S. Yla-Herttuala, "VEGF Gene Transfer Reduces Intimal Thickening via Increased Production of Nitric Oxide in Carotid Arteries," *Human Gene Therapy*, vol. 8, pp. 1737-1744, 1997.

[103] M. Laitinen, K. Makinen, H. Maninen, ... and S. Yla-Herttuala, "Adenovirus-Mediated Gene Transfer to Lower Limb Artery of Patients with Chronic Critical Leg Ischemia," *Human Gene Therapy*, vol. 9, pp. 1481-1486, 1998.

[104] S. Rajagopalan, E. Mohler III, R. Lederman, ... and B. Annex, "A Phase II Randomized, Double-Blind, Controlled Study of Adenoviral Delivery of Vascular Endothelial Growth Factor 121 in Patients with Disabling Intermittent Claudication," *Circulation* , vol. 108, pp. 1933-1938, 2003.

[105] Y. Kusumanto, V. Van Weel, N. Mulder, ... and G. Hospers, "Treatment with Intramuscular Vascular Endothelial Growth Factor Gene Compared with Placebo for Patients with Diabetes Mellitus and Critical Limb Ischemia: A Double-Blind Randomized Trial," *Human Gene Therapy,* vol. 17, pp. 683-691, 2006.

[106] S. Iyer and B. Annex, "Therapeutic Angiogenesis for Peripheral Artery Disease," *JACC: Basic to Translational Science,* vol. 2, no. 5, pp. 503-512, 2017.

[107] F. G. R. Fowkes and J. Price, "Gene therapy for critical limb ischaemia: the TAMARIS trial," *The Lancet,* vol. 377, no. 9781, pp. 1894-1896, 2011.

[108] H. Shigematsu, K. Yasuda, T. Iwai, ... and R. Morishita, "Randomized, double-blind, placebo-controlled clinical trial of hepatocyte growth factor plasmid for critical limb ischemia," *Gene Therapy,* vol. 17, pp. 1152-1161, 2010.

[109] R. Powell, M. Simons, F. Mendelsohn, ... and B. Annex, "Results of a double-blind, placebo-controlled study to assess the safety of intramuscular injection of hepatocyte growth factor plasmid to improve limb perfusion in patients with critical limb ischemia," *Circulation,* vol. 18, no. 1, pp. 58-65, 2008.

[110] H. L. Huang, N. Wang, H. Zhou and C. Y. Yu, "Study on influence of transient ischemic attack," *European Review for Medical and Pharmacological Sciences,* vol. 20, pp. 5164-5167, 2016.

[111] C. Murry, R. Jennings and K. Reimer, "Preconditioning with ischemia: a delay of lethal cell injury in ischemic myocardium," *Circulation,* vol. 74, no. 5, pp. 1124-1136, 1986.

[112] C. Peralta, A. Serafin, L. Fernandez-Zabalegui, Z. Y. Wu and J. Rosello-Catafau, "Liver Ischemic Preconditioning: A New Strategy for the Prevention ofIschemia-Reperfusion Injury," *Transplant Proceedings,* vol. 35, pp. 1800-1802, 2003.

[113] N. Mewton, T. Bochaton and M. Ovize, "Postconditioning the Heart of ST-Elevation Myocardial Infarction Patients," *Circulation Journal,* vol. 77, no. 5, pp. 1123-1130, 2013.

[114] T.-T. Cung, O. Morel, G. Cayla, ... and M. Ovize, "Cyclosporine before PCI in Patients with Acute Myocardial Infarction," *New England Journal of Medicine,* vol. 373, no. 11, pp. 1021-1031, 2015.

[115] H. Tsubota, A. Marui, J. Esaki, S. C. Bir and R. Sakata, "Remote Postconditioning may AttenuateIschaemiaeReperfusion Injury in the MurineHindlimb Through Adenosine Receptor Activation," *European Journal of Vascular & Endovascular Surgery ,* vol. 40, pp. 804-809, 2010.

[116] G. Amit, C. Cafri, S. Yaroslavtsev, ... and D. Zahger, "Intracoronary nitroprusside for the prevention of the no-reflow phenomenon after primary percutaneous

coronary intervention in acute myocardial infarction. A randomized, double-blind, placebo-controlled clinical trial," *American Heart Journal,* vol. 152, no. 5, pp. 887.e9-887.e14, 2006.

[117] H. Öhlin, N. Pavlidis and A.-K. Öhlin, "Effect of intravenous nitroglycerin on lipid peroxidation after thrombolytic therapy for acute myocardial infarction," *The American Journal of Cardiology,* vol. 82, no. 12, pp. 1463-1467, 1998.

[118] L. D. Sun, Y. L. Tang, W. B. Xi, N. Zhang and Y. Z. Zhang, "Study on the reperfusion rate of acute myocardial infarction affected by inspiring nitric oxide and resolving thrombus intravenously before admission," *Zhongguo wei Zhong Bing ji jiu yi xue,* vol. 16, no. 3, pp. 169-171, 2004.

[119] M. Mathru, R. Huda, D. Solanki, S. Hays and J. Lang, "Inhaled Nitric Oxide Attenuates Reperfusion Inflammatory Responses in Humans," *Anesthesiology,* vol. 106, pp. 275-282, 2007.

[120] S. Dragoni, T. Gori, M. Lisi, G. Di Stolfo, A. Pautz, H. Kleinert and J. Parker, "Pentaerythrityl Tetranitrate and Nitroglycerin, but not Isosorbide Mononitrate, Prevent Endothelial Dysfunction Induced by Ischemia and Reperfusion," *Arteriosclerosis, Thrombosis, and Vascular Biology,* vol. 27, pp. 1955-1959, 2007.

[121] P. Botha, M. Jeyakanthan, J. Rao, A. Fisher, M. Prabhu, J. Dark and S. Clark, "Inhaled Nitric Oxide for Modulation of Ischemia–Reperfusion Injury in Lung

Transplantation," *The Journal of Heart and Lung Transplantation,* vol. 26, no. 11, pp. 1199-1205, 2007.

[122] D. Cornfield, C. Milla, I. Haddad, J. Barbato and S. Park, "Safety of Inhaled Nitric Oxide AfterLung Transplantation," *The Journal of Heart and Lung Transplantation,* vol. 22, no. 8, pp. 903-907, 2003.

[123] K. Arom, D. Angaran, W. Lindsay, W. Northrup and D. Nicoloff, "Effect of Sodium Nitroprusside during the Payback Period of Cardiopulmonary Bypass on the Incidence of Postoperative Arrhythmias," *The Annals of Thoracic Surgery,* vol. 34, no. 3, pp. 307-312, 1982.

[124] M. Asgharpour, A. Tolouian, L. Bhaskar, R. Tolouian and N. Massoudi, "Herbal antioxidants and renal ischemic-reperfusion injury; an updated review," *Journal of Nephropharmacology,* vol. 10, no. 1, 2021.

[125] J. Flaherty, B. Pitt, J. Gruber, ... and S. Werns, "Recombinant Human Superoxide Dismutase (h-SOD) Fails to Improve Recovery of Ventricular Function in Patients Undergoing Coronary Angioplasty for Acute Myocardial Infarction," *Circulation,* vol. 89, no. 5, pp. 1982-1991, 1994.

[126] K. Tsujita, H. Shimomura, H. Kawano, ... and H. Ogawa, "Effects of edaravone on reperfusion injury in patients with acute myocardial infarction," *The American Journal of Cardiology,* vol. 94, no. 4, pp. 481-4848, 2004.

[127] P. Pacher, J. Beckman and L. Liaudet, "Nitric oxide and peroxynitrite in health and disease," *Physiological Reviews,* vol. 87, no. 1, pp. 315-424, 2007.

[128] R. Radi, "Oxygen radicals, nitric oxide, and peroxynitrite: Redox pathways in molecular medicine," *Proceedings of the National Academy of Sciences of the United States of America,* vol. 115, no. 23, pp. 5839-5848, 2018.

[129] M. Feelisch, J. Ostrowski and E. Noack, "On the Mechanism of NO Release from Sydnonimines," *Journal of Cardiovascular Pharmacology,* vol. 14, pp. S13-S22, 1989.

[130] C. Wilcox, "Effects of tempol and redox-cycling nitroxides in models of oxidative stress," *Pharmacology & Therapeutics,* vol. 126, no. 2, pp. 119-145, 2010.

[131] B. Koppolu, M. Rahimi, S. Nattama, A. Wadajkar and K. Nguyen, "Development of multiple-layer polymeric particles for targeted and controlled drug delivery," *Nanomedicine,* vol. 6, no. 2, pp. 355-361, 2010.

[132] B. Shah, S. Kona, T. Gilbertson and K. Nguyen, "Effects of Poly-(lactide-co-glycolide) Nanoparticles on Electrophysiological Properties of Enteroendocrine Cells," *Journal of Nanoscience and Nanotechnology,* vol. 11, pp. 3533-3542, 2011.

[133] J. Menon, P. Ravikumar, A. Pise, D. Gyawali, C. Hsia and K. Nguyen, "Polymeric Nanoparticles for Pulmonary Protein and DNA delivery," *Acta Biomater,* vol. 10, no. 6, pp. 2643-2652, 2014.

[134] R. Crawford, F. Hashmi, J. Jones, H. Albadawi, M. McCormack, K. Eberlin, F. Entabi, M. Atkins, M. Conrad, W. Austen and M. Watkins, "A novel model of

acute murine hindlimb ischemia," *American Journal of Physiology-Heart and Circulatory Physiology,* vol. 292, pp. H830-H837, 2007.

[135] R. Brenes, C. Jadlowiex, M. Bear, P. Hashim, C. Protack, X. Li, W. Lv, M. Collins and A. Dardik, "Toward a mouse model of hind limb ischemia to test therapeutic angiogenesis," *Journal of Vascular Surgery,* vol. 56, no. 6, pp. 1669-1679, 2012.

[136] T. Kochi, Y. Imai, A. Takeda, Y. Watanabe, S. Mori, M. Tachi and T. Kodama, "Characterization of the Arterial Anatomy of the Murine Hindlimb: Functional Role in the Design and Understanding of Ischemia Models," *PLOS ONE,* vol. 8, no. 12, 2013.

[137] V. Kumar, N. Wickremasinghe, S. Shi, T. Cornwright, Y. Deng, ... and J. Hartgerink, "Treatment of hind limb ischemia using angiogenic peptide nanofibers," *Biomaterials,* vol. 98, pp. 113-119, 2016.

[138] E. Fernandes, S. Toste, J. Lima and S. Reis, "The Metabolism of Sulindac Enhances its Scavenging Against Reactive Oxygen and Nitrogen Species," *Free Radical Biology & Medicine,* vol. 35, no. 9, pp. 1008-1017, 2003.

[139] X.-T. Ma, Z.-Y. Sun, K. Yu, B.-S. Gui, Q. Gui and J.-M. Ouyang, "Effect of Content of Sulfate Groups in Seaweed Polysaccharides on Antioxidant Activity and Repair Effect of Subcellular Organelles in Injured HK-2 Cells," *Oxidative Medicine and Cellular Longevity,* 2017.

[140] H. T. R. Katsumi, H. Suzuki and A. Yamamoto, "S-nitrosylated L-serine-modified dendrimer as a kidney-targeting nitric oxide donor for prevention of renal ischaemia/reperfusion injury," *Free Radical Research,* pp. 1-7, 2019.

[141] V. Kleshchevnikov, A. Shmatko, E. Dann, ... and O. Bayraktar, "Comprehensive mapping of tissue cell architecture via integrated single cell and spatial transcriptomics," *Frontiers in Immunology,* 2020.

[142] K. Kokolus, Y. Zhang, J. Sivik, ... and T. Schell, "Beta blocker use correlates with better overall survival in metastatic melanoma patients and improves the efficacy of immunotherapies in mice," *Oncoimmunology,* 2017.